Albedometer Design:

Improving the Accuracy, Functionality and Usability of the TUDelft Spectrally Resolved Albedometer

SET3901: Graduation Project

Lucas Bungay

Delft University of Technology

TU Delft

Albedometer Design:

Improving the Accuracy, Functionality and Usability of the TUDelft Spectrally Resolved Albedometer

by

Lucas Bungay

Student Name	Student Number
Lucas Bungay	5581923

Chair:	Prof.Dr.Ir. A.H.M Smets	PVMD group
External Member:	Dr. A. Lekic	IEPG group
Supervisor:	Dr. H. Ziar	PVMD group
Assisting Supervisor:	Ir. A. Martinez Lopez	PVMD group
Thesis Defence Date:	16th October 2023	
Faculty:	Faculty of Electrical Engineering, Mathematics and Computer Science, Delft	

TU Delft

Preface

These two years studying Sustainable Energy Technology have been unforgettable. First arriving in the Netherlands, I am full of anticipation for beginning of this new chapter, for the new studies I am undertaking and for the people that I would meet. My expectations were far exceeded. The privilege of studying in the field of sustainable energy have equipped me with the skills I need make a real difference amidst the climate crisis we are facing today. To my friends I have met here, never would I have expected to find my place so quickly amongst so many intelligent, kind and open-minded people who allowed me to discover, and truly be myself. I look forward to the many more memories we will create together. To my friends abroad, I thank you for your friendship and support. Despite the distance, I never feel very far from you at all.

That I am able to have completed this thesis successfully and with such dedication, is thanks to my daily supervisor Hesan Ziar, and assisting supervisor, Arturo Martinez Lopez. I would like to thank Hesan, for our regular meetings where our discussions have taught me much about much about the scientific research community, inspiring me to create a piece of work I can truly be proud of. Your support and insightful feedback have been invaluable to me. To Arturo, I am grateful for your challenging questions which have helped me to explore the technicalities of the project, for your helping hand and Python coding prowess. Thank you!

Last but not least, I would like to thank my family. To my family in France who, through covert family communication lines, somehow always know what's on my mind, your encouraging words have given me the confidence I need to manoeuvre any challenge. To my sister, our regular chats and the updates of your energetic actress lifestyle never cease to make my day, knowing that you too are exploring your passion. I would like to thank my parents, your continual love and support has always encouraged me to pursue my passions, enabling me to be as happy and fulfilled as I am today.

Lucas Bungay
Delft, November 2023

Abstract

The TUDelft spectrally resolved albedometer is a measurement device whose design began in 2019 and aims to accurately reconstruct spectral irradiance and spectral albedo using reconstruction techniques which enable this device to be produced at a lower cost than its competitors.

The measurement of spectral albedo using an albedometer device is a crucial component in predicting energy yield for bifacial PV panels, expected to become the dominant photovoltaic technology by market share in 2030 [13]. Building on the work of previous thesis projects at TUDelft, this thesis focuses on the following three topics of improvement:

Accuracy improvement in spectral reconstruction: The albedometer device is recalibrated according to the recently recalibrated EKO device, succeeding in reducing the error uncertainty in the first and last wavelength ranges of the spectral irradiance reconstruction. Whilst the average errors lie outside of acceptable uncertainty bounds, the systematic errors in the first and last wavelength bands are identified and proposed solutions involve adjusting the PSO algorithm and using machine learning to improve the prediction of atmospheric absorption parameters such as total precipitable water.

Spectral albedo reconstruction using Machine Learning: Machine learning techniques are employed to reconstruct down-facing spectral irradiance, achieving errors below $\pm$5% for various sky classes and demonstrating the method's potential for spectral albedo reconstruction in future work.

Improving device usability: The Albedometer App centralizes and automates data processing code, simplifying spectral irradiance and albedo reconstruction processes and greatly enhancing user experience.

This research is key for the development for the albedometer's accuracy, functionality and usability. By integrating the model for spectral albedo reconstruction this thesis advances the overall development of the albedometer device, bring it one step closer to realising its full potential as a high accuracy, low cost measurement device, making it a valuable tool for spectral albedo reconstructions and precise energy yield predictions in the bifacial PV sector.

Contents

Nomenclature

Abbreviations

Abbreviation	Definition
UHI	Urban Heat Island
PSO	Particle Swarm Optimisation
PCB	Printed Circuit Board
nm	Nanometer
Kc	Clear Sky Index
ML	Machine Learning
PV	Photovoltaic
GPR	Gaussian Process Regression
RF	Random Forest (modelling)
AI	Artificial Intelligence
MSE	Mean Squared Error
SMARTS	Simple Model of the Atmospheric Radiative Transfer of Sunshine
SC	Skyclass
UFSI	Upward-facing Spectral Irradiance
DFSI	Downward-facing Spectral Irradiance

1

Introduction & Literature Review

Climate change and sustainability are paramount global concerns. In 2015, under the Paris agreement, the United Nations signed an international treaty on climate change which strives to limit the average global temperature to 1.5°C above pre-industrial levels. Recent IPCC reports have shown that the 1.5°C limit can be reached in as little as two decades [19]. The need for renewable energy sources has never been more important.

Solar energy emerges as a pivotal player in the quest to achieve these renewable energy goals and combat climate change. Solar power, harnessed from the sun's abundant and renewable rays, offers an environmentally friendly and sustainable alternative to fossil fuels. Bifacial photovoltaic (PV) systems have gained significant traction in recent years and according to the International Technology Roadmap for Photovoltaic [13], bifacial modules are set to become dominant photovoltaic technology by market share in 2030, see figure 1.1. The development of cost-effective albedometer devices capable of accurately measuring spectral albedo, harbors significant potential, not only to contribute to advancing bifacial PV technology but also to aid in monitoring the Earth's response to global warming by assessing changes in surface reflectivity, see section 1.1. By supporting the implementation of bifacial PV and aiding in climate change tracking, the albedometer play a vital role in driving the transition towards a more sustainable future.

This thesis consists of the following chapters, with the research questions detailed in section 1.5. In this chapter, chapter 1, a literature review is provided on spectral albedo and its practical applications, along with an introduction to the TUDelft albedometer and project background. In chapter 2, the methodology of the project is outlined, explaining the steps taken to address three key research questions: improving the accuracy of spectral irradiance reconstruction, developing a model for spectral albedo reconstruction, and designing the Albedometer App. In chapter 3, the results for each of the aforementioned research questions are presented, followed by in-depth discussions of these findings. The conclusion can be found in chapter 4, and recommendations for future work are outlined in chapter 5.

1.1. Bifacial PV and Applications of Spectral Albedo

Bifacial Photovoltaics (PV), unlike conventional monofacial PV modules, are capable of converting solar energy into electricity on both side of the device, thereby being capable of generating more power. Bifacial PV has been shown to increase the power production of some of the typical configurations of PV systems. Bifacial modules attached to a sun tracker in Madrid, Spain, generated 1.7 times the annual energy yield of that with a monofacial panel [27] and the configuration of bifacial module in rows as though in a PV plant, increases the energy yield by 110% compared to monofacial modules for optimal correct packing factor and panel tilt [6].

An additional strength of bifacial PV is in the vertical configuration. Whilst it has been shown that tilted bifacial PV panels may produce 32% more energy than vertical bifacial PV panels, more vertical collectors can be installed for the same field size [1]. There is also a large potential for vertical and tilted

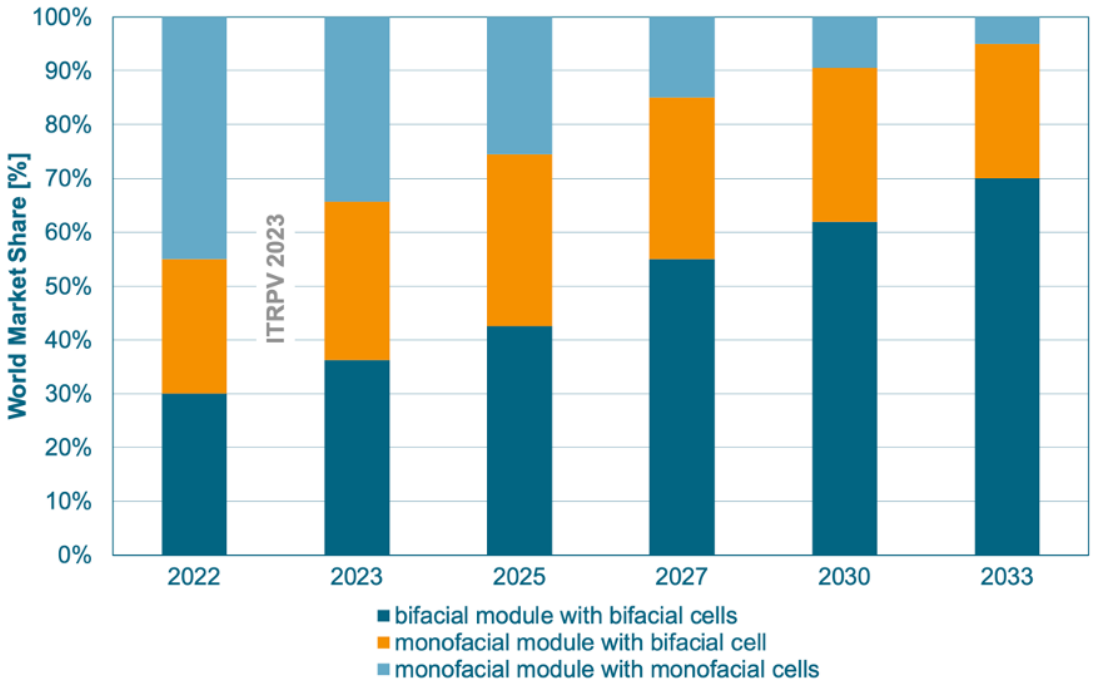

Figure 1.1: Predicted world market share for monofacial and bifacial modules. Bifacial cells are expected to exceed 60% market share by 2030.

bifacial PV in the field of Agrivoltaics, the study of how solar energy and crop production can mutually fulfil growing food and energy demands. A study on vertical bifacial module orientation over a crop producing field found that the panels in the East-West orientation preserved > 80% of the crop yield and reduced water demand of the crops due to increased shading during harsh weather conditions [28].

In each of the aforementioned bifacial PV projects and model, spectral albedo is of utmost importance for energy yield predictions where ground reflected radiation is reported to contribute approximately 10% of the effective irradiance received by bifacial systems compared to the approximately 3% for monofacial systems [29][26]. Spectral albedo, the measure of reflected light across different wavelengths, as a percentage of the total up-facing spectral irradiance, is a vital component of bifacial irradiation modelling - required to calculate the energy yield of a bifacial system. Spectral albedo is further explored in the next section, section 1.2.

The use of spectral albedo is not unique to bifacial PV, and is also be used as in indicator for local and global warming as measured by the heat island effect, as an indicator for wildlife conservation, particularly in polar regions and for remote sensing.

The urban head island (UHI) effect is a well documented phenomenon, that the temperatures around cities and urbanised areas are increased due to the manmade structures such as buildings and roads which absorb heat differently to the natural landscapes of forest and water bodies [35]. Studies have used spectral albedo to measure how increasing material's spectral reflectivity in the urban environment, such as in concrete roads [22] and ceramic tiles on roofs [5] can be used to mitigate the effect of UHI. The reduction of UHI locally has a wider effect on global warming, considering the challenges of increasing urbanisation, every increase of local warming contributes in part to the global warming of the planet [35][36]. Spectral albedo therefore is an important indicator of increasing reflectivity within the urban environment, but also plays a part in the research for UHI effect mitigation.

In wildlife conservation, the spectral albedo is commonly used in polar regions. Since snow is the "brightest substance of considerable extent on the surface of our planet and, because of its high albedo compared to other natural surfaces" [24], the seasonal fluctuations of the the earth's ice sheets has a

significant effect upon the average albedo of the planet. Tracking of the seasonal fluctuations of ice-sheets using spectral albedo also relates to the remote sensing application of an albedometer sensor. Spectral albedo has also been used to to measure contamination of the snow due to pollutants in the atmosphere, not only to measure the quality of the snow and ice but as a measure of global emissions affecting nature [9][15].

1.2. Spectral Albedo

Spectral albedo is a measure of reflected light across different wavelengths, quantifying the fraction of incoming radiation that is reflecting back into the atmosphere. Spectral albedo changes daily according to the time of day and position of the sun, but the reflected component of albedo means that it is also affected by the changing geometry of the environment at different times of day [36]. The measurement of spectral albedo also changes seasonally and due to weather conditions. On a shorter timescale, a wet ground changes the reflectivity of the material significantly to that in dry conditions and the reflectivity of snowy ground in seasonal changes varies greatly [2].

The basis for the spectral albedo modelling in this thesis is the equation developed by H. Ziar in 2019 [36] which mathematically models how the geometry of shadows, material spectral features and temporal changes affect the spectral albedo. The equation for spectral albedo is given as:

$$\alpha(\lambda) = \sum_{i=1}^{i=N} R_i(\lambda) \left(C_i F_{S \to A_{i1}} + \frac{1}{H+1} \left(C_i^{'} F_{S \to A_{i1}} + F_{S \to A_{i2}} \right) \right) \tag{1.1}$$

A detailed derivation is carried out in the original paper to arrive at this equation. The layout of surfaces highlighted in this equation are visualised in figure 1.2. To explain the components of equation (1.1), it is first assumed that the point at which spectral albedo, $\alpha(\lambda)$ is desired, lies on the surface S (depicted as the albedometer) which lies above the surface of the ground, A. $R_i(\lambda)$ represents the reflectivity of the ground and the factor H models the effect of solar position and sky conditions, as given by equation (1.2), where surface M is parallel to surface S and the point at which DNI and DHI are measured.

$$H = \frac{DNI_M}{DHI_M} cos(\theta_M) \tag{1.2}$$

In equation (1.1), $F_{S \to A_{i1}}$ and $F_{S \to A_{i2}}$ are the view factors of shaded and unshaded parts of the ground, as viewed by the down facing side of surface S. C_i and $C_i^{'}$ represent the roughness of the ground, where C_i is the chance (probability) that the unshaded surface A_{i1} is illuminated, and visible to the surface S and $C_i^{'}$ is the chance that the unshaded surface A_{i1} is visible to surface S but not illuminated.

To summarise, the equation for spectral albedo is a function of the spectral reflectivity and roughness of the ground, the view factor of shaded and unshaded parts of the ground, the solar position and sky conditions at the time of measurement.

1.3. About the Albedometer

The TU Delft spectrally resolved albedometer is a measurement device capable of measuring irradiance in three bands between 320nm and 1100nm. The device features six photosensitive diodes (sensors)[1] split between the top and bottom of the device. The layout of the sensors is symmetrical on the top and bottom. The 3D printed bio-inspired casing separates top and bottom sensors, preventing light on one side from affecting the measurements of the other. Light enters through hybrid diffusers which diffuse light as evenly as possible inside the device. The scattered light inside the device is then measured by the sensors, each capable of detecting light in the ranges of 320nm to 1100nm. Two of the three sensors are covered by long-pass filters which limit the wavelengths of light passing through them. The sensors therefore measure irradiance in the wavelengths ranges shown in table 1.1. The device is also equipped with a temperature sensor in the top and bottom sections to enable temperature calibration, and identification of possible short circuits which may cause overheating in the device.

[1] 'Photosensitive diodes', 'photodiodes' and 'sensors' are used interchangeably in this report.

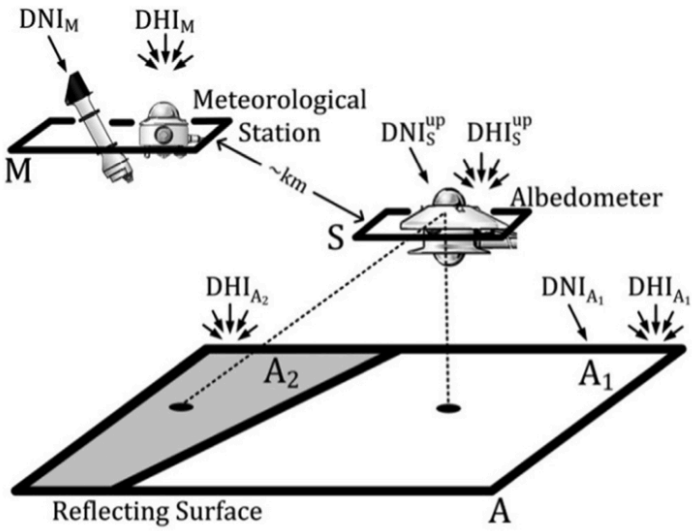

Figure 1.2: Layout of surfaces to visualise equation (1.1). Surface S is parallel to surface M while the surface A is not necessarily. The angle of incidence between sunlight rays and the surface S, θ_S and M, θ_M are equal but not necessarily equal to that of surface A, θ_A [36]

The albedometer begins recording data when it's data collection software is turned on manually via the computer at the PVMD monitoring roof. Continual measurements are taken every second and recording is stopped manually, during normal operation, or automatically, when an error occurs. Data files, in .csv format, can therefore contain weeks worth of data, resulting in large datasets, greater than 100MBs. At each timestep, the albedometer records: the date and time, the irradiance measured by the sensors, and the internal temperature of both sides of the device. Sample albedometer data can be found in appendix A

The spectral reconstruction of the top-side of the device was developed in 2020 by W. Meines [23]. The reconstruction uses SMARTS2, a spectral radiation model which "can be used in a variety of applications to predict full terrestrial spectra under any cloudless atmospheric condition" [7]. The measurements of the three top-side sensors are used to determine the irradiance in the three wavelength bands required by SMARTS, see table 1.2. The model outputs the spectral reconstruction in the range of 320-1100nm with wavelength interval of 0.5nm between 320nm and 400nm and 1nm between 400nm-1100nm.
The albedometer is mounted to a 'SOLYS 2' sun tracker on the PVMD monitoring roof which follows the position of the sun whilst keeping the equipment horizontal [37], see figure 1.3. Mounted alongside it are the EKO MS-700 Spectroradiometer and two pyranometers. The EKO MS-700, built by EKO Intruments Co., Ltd, can measure spectral irradiance values in the range of 320-1100nm with wavelength intervals of 3.2nm [3]. The spectral irradiance measured by the EKO device is used as a reference for the error analysis shown in this paper.

1.4. Previous Thesis Work

Work on TUDelft's spectrally resolved albedometer first began in 2019. A. Kaul, designed and fabricated an irradiance sensor [18] featuring three photosensitive diodes on the top and bottom of the device, see figure 1.4a, which took instantaneous readings of the output current and converted them into irradiance measurements. The three irradiance sensors measured in the wavelength bands of 300nm to 1100nm and were split into three wavelength bands using optical filters. In the full wave-

Table 1.1: Wavelength ranges measured by the albedometer sensors.

Sensor Number	Sensor 1	Sensor 2	Sensor 3
Wavelength range (nm)	320-1100	590-1100	850-1100

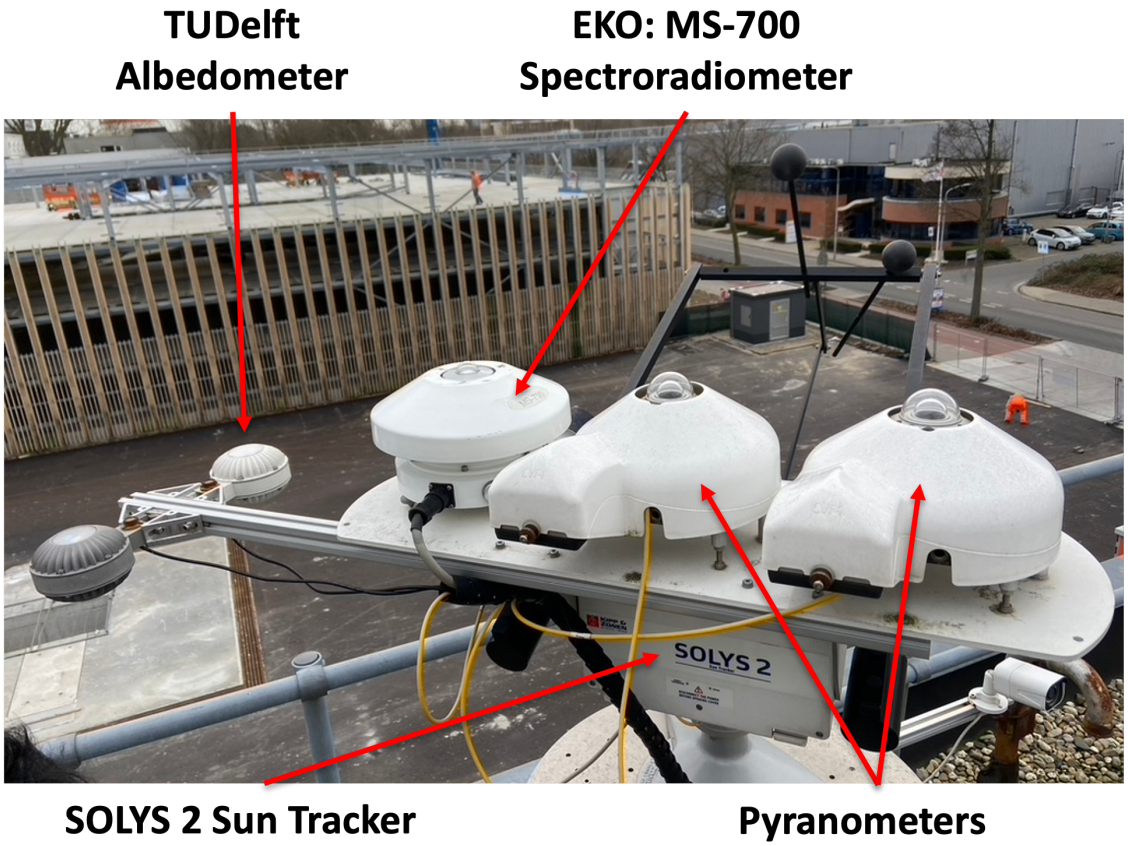

Figure 1.3: Installation of albedometer and EKO device on PVMD monitoring roof.

length range, the irradiance measurement error relative to the reference EKO device was 14.15%.

In the second project, A.R.Olvera improved the accuracy of the device by experimenting with the optical design of the device as well as the electrical and mechanical design [25]. In the optical design, new diffusers and filters were tested. The diffusers were changed from N-BKT diffusers to hybrid diffusers due to their superior scattering properties at high wavelengths. Long-pass optical filters were selected as the primary filter type due to their lower price and sharper cut-off wavelengths relative to the hot-mirror filter used in the previous irradiance sensor. Furthermore, long-pass filters are widely available and can be easily integrated if an additional sensor is placed in the future.

The albedometer PCB was redesigned to better fit the device's casing and to improve the reliability of data transfer from the device via the cable. The additional function of the bio-inspired casing design was to reduce the internal operating temperatures of the device by mimicking the high surface area of a cactus, allowing heat to dissipate easily to the surroundings, see figure 1.4b. The white 3D printed casing demonstrated operating temperatures of 2°C less than the first, non-ribbed design.

Based on the temperature dependency of the sensors' readings, A. Romero also developed a temperature calibration method. Temperature coefficients were calculated for each sensor and used to correct the sensors' readings based on the difference between the external temperature and the inter-

Table 1.2: Wavelength bands required by SMARTS.

Band 1	Band 2	Band 3
320-590nm	590-850nm	850-1100nm

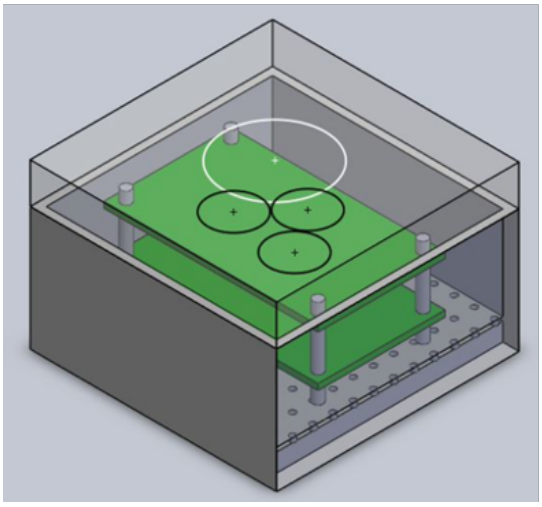

(a) First iteration of irradiance sensor [18].

(b) Bio-Inspired design of albedometer [25]

nal temperature of the device. Following implementation of the improvements discussed above, the final measured relative error in the full wavelength range was 7.3%.

Finally, in 2022 W. Meines designed a reconstruction model which ”simulates clear-sky solar spectra with limited irradiance inputs from a spectrally resolved albedometer” [23] based on SMARTS2 spectral irradiance model [7]. In this thesis, W. Meines uses measurements from the three sensors of the albedometer, to reconstruct the top-side irradiance of the device. Competitor devices, such as the Spectrafy SolarSIM:ALB [32] feature additional irradiance sensors placed at specific wavelengths in order to isolate the atmospheric parameters that determine the precise shape of the reconstructed spectrum. The TUDelft albedometer determines these values instead using Particle Swarm Optimisation (PSO), which solves for the optimal values of three atmospheric parameters which most affect the spectrum in the 320nm to 1100nm range: aerosol optical depth at 550nm, ozone reduced pathlength and total precipitable water.

The final reconstruction errors as compared to the reference EKO device in each of the three measured wavelength bands, can be found in table 1.3.

Table 1.3: Absolute and relative errors of spectral reconstructions in each wavelength range [23]. The ’Range’ rows indicate the range of the 95% confidence interval.

		Wavelength range [nm]			
		320-590	590-850	850-1100	Total (320-1100)
Absolute error [W/m^2/nm]	Range	[-0.055, 0.043]	[-0.021, 0.032]	[-0.022, 0.029]	[-0.033, 0.035]
	Mean	-0.008	0.010	0.004	0.002
Relative error [%]	Range	[11.3, 9.1]	[-2.1, 4.9]	[-4.6, 10.1]	[-6.2, 8.2]
	Mean	-1.9	2.1	2.3	0.82

1.5. Research Aims and Project Scope

The global aim of this project is to create an accurate, cost-effective, and easy-to-use albedometer device. In pursuit of this objective, the project has been divided into three distinct sections, outlined in the following research questions:

1. **Can the recalibration of the albedometer improve the error measurements of the device or is a physical change to the device required?**
2. **Can a model be built to reconstruct spectral albedo using the data available to the device?**
3. **How can a user interface be designed which simplifies user experience for spectral irradiance and albedo reconstruction?**

To answer the first research question, the recommendations from the previous thesis [23] must be investigated. To conclude the work of W. Meines, the uncertainties of the spectral irradiance reconstruction model were compared to those reported of the reference EKO device, see table 1.4. The uncertainty of the EKO device is reported in the calibration certificate of the July 2022 recalibration. It is observed that in the first and last wavelength ranges in table 1.4, the albedometer spectral reconstruction violates the uncertainty bounds by 0.5% and 8% respectively. Three recommendations are suggested to address the violation of the uncertainty bounds:

1. Repeat error analysis with recalibrated EKO and albedometer.
2. Aerosol transmittance and trace gas investigation.
3. Place additional sensors.

It was suspected that the EKO device had become uncalibrated with time, which in turn, affected the calibration of the Albedometer device. In this research, the spectral irradiance reconstructions are repeated with the newly calibrated reference device, to analyse how the relative errors in each wavelength band are affected. The next recommendation suggests that finding the optimal values of Trace gas and Aerosol transmittance in the SMARTS reconstruction may reduce the error in the region of 320-590nm , especially below 499nm, where the coefficients for aerosol transmittance change [23]. Finally, should neither of these recommendations work, the placing of an additional sensor can be considered.

Table 1.4: Reconstruction errors vs EKO reported uncertainties [23].

	Wavelength range [nm]		
	350-450	450-900	900-1050
Reconstruction 95% error range [%]	[-11.62, 11.87]	[-3.92, 3.73]	[-3.3, 12.75]
Reconstruction mean error [%]	-1.43	0.43	4.07
EKO uncertainty [%]	$\pm$ 11.35	$\pm$ 5.00	$\pm$ 4.39

The second research question aims to design a model for reconstructing spectral albedo. A key design requirements of the albedometer referenced in this project, is the capability to reconstruct spectral irradiance and spectral albedo within a certain error margin. A machine learning method will be employed to help predict the down-facing spectral irradiance (DFSI) using minimal external inputs. The research question will be answered by analysing the error of the reconstruction relative to its reference DFSI, then comparing it to the relative error of our competitor device, the Spectrafy SolarSIM:ALB, < 5% $\pm$ 0.05 W/m^2 per wavelength [31]. The results of the reconstruction of DFSI will demonstrate the potential for ML reconstruction of the Spectral Albedo in future work.

The third research question relates to the development of a user interface which simplifies the use of the albedometer device spectral reconstruction. In this section, the target audience is identified, based on the literature review in section 1.2 and the design requirements of the app are determined. The app is developed using MATLAB app designer.

2

Methodology

2.1. Data Collection & Preparation

2.1.1. Sky Classification Data Gathering

Using the sky classification model, developed by G. van Urk in 2022 [33] and later improved by V.A. Martinez Lopez et al. [21], sky images of Delft can be analysed and sorted into 5 different sky classes, depending on their clear sky index (K_c) and cloud cover. Clear sky index, K_c is the "ratio of measured irradiance at ground level to estimated irradiance in clear sky conditions at ground level" [17]. At low elevations and in partly cloudy conditions, it is possible for K_c to exceed 1, this is due to the cloud enhancement effect, where photons are scatted by water droplets in the direction of the sensor and measured as direct irradiance [16]. Cloud cover is the proportion of the sky which is covered by clouds, where 0, is a cloudless sky and 1 is an overcast sky. The sky images are processed and categorised into different Skyclasses, as indicated by table 2.1

A sky camera is installed near the albedometer which captures sky images at the top of each minute. The sky classification code was run for all sky images between September 2022 and May 2023. The data is then used for error analysis in the top-side spectral reconstructions of the albedometer, section 3.1 and spectral reconstruction of albedo, section 3.2 . Figure 2.1 shows the SkyClass data of all the reconstructed points as well as their clear sky index and cloud cover values.

Sample data from the sky classification code can be found in appendix A.

Table 2.1: SkyClass category separation as determined by K-means data clusters for clear sky index (K_c) and cloud cover (CC) values [21].

Skyclass (SC)	Sky condition	Clear Sky Index (K_c) & Cloud Cover (CC)
1	Clear-sky	High K_c, Very low CC
2	Partly cloudy	Lower K_c and Higher CC relative to SC 1
3	Overcast with high irradiance	High K_c, High CC
4	Overcast	Very low K_c, Very high CC
5	Partly clear skies with obscured sun	Low K_c, Low CC

2.1.2. Albedometer Data Timeline

Albedometer data, is the raw data collected by the albedometer device. As previously mentioned in section 1.3, the files can contain weeks worth of data, resulting in large datasets greater than 100MBs. Consequently, loading, reading and processing the datafiles from the albedometer and EKO device is computationally time-consuming. In addition, the times at which the data coincide with one another is unclear and sorting though the data to find relevant information is time consuming. Improved understanding of the quantity and contents of available data files would help to select relevant and usable files for reconstructions and error analyses. The first task is therefore to visualise the available data by

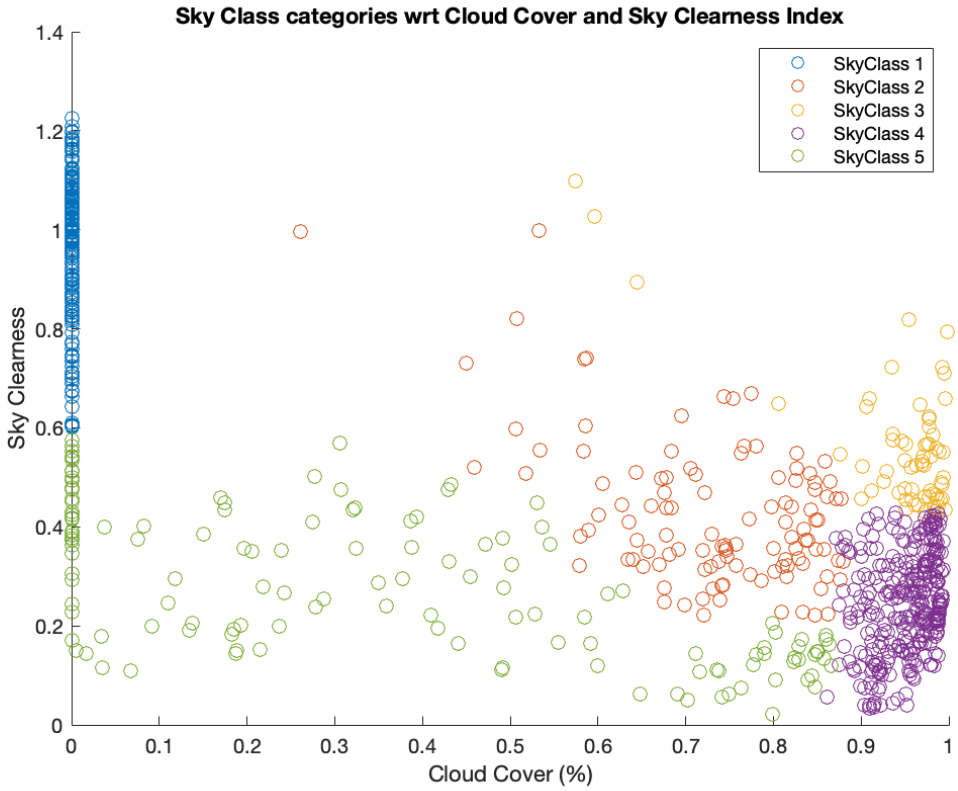

Figure 2.1: SkyClass, clear sky index and cloud cover of datapoints for which the spectrum was reconstructed.

creating a timeline.

The EKO device measures data from 6am to 10pm every day at 1 minute intervals. Raw EKO data comes in two files, 'specoverview' and 'specdata'. The 'specdata' files store the irradiance data for each of the 255 measured wavelengths, ranging from 300nm to 1150nm, whilst the 'specoverview' files indicate the indexes of the 'specdata' files which refer to a specific date and time.

To create the timeline, a Python scipt was written, which extracted the start and end times of each albedometer and EKO data files, sorting them into chronological order alongside their respective filenames. The timeline also includes the range of times for which sky classification analysis was performed, as well as a timeline of which EKO devices were in operation. The full timeline is shown in figure 2.2.

Sample data for Albedometer and EKO data can be found in appendix A.

To perform reconstructions and error analysis, the following data must be met: Albedometer data must be available to run the spectral reconstructions, EKO data must be available to compare the reconstructed data to the real values and sky classification data must be available to provide insight as to what sky conditions are causing certain errors. Since only EKO 1 was recalibrated, we may only use the EKO data for when EKO 1 is installed. We can therefore determine the following usable dates given the constraints:

- 7th to 30th September, 2022
- 1st to 30th November, 2022
- 1st to 17th February 2023

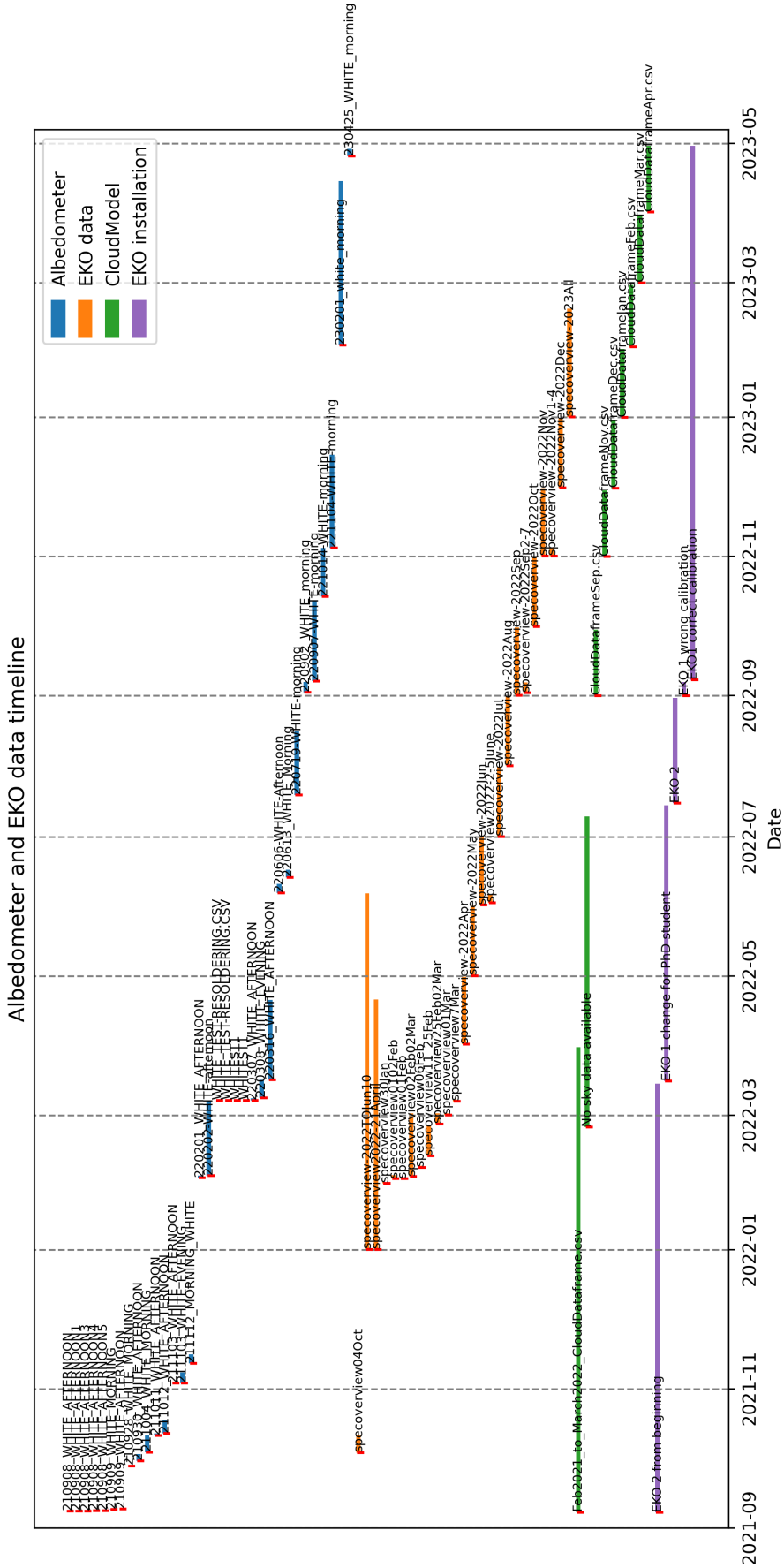

Figure 2.2: Timeline for project data. Provides information about the dates for which albedometer, EKO and CloudModel data is available, as well as information about which EKO was in operation. The names next to each bar is purposefully kept and is used to identify the names of datafiles in which the desired data is stored.

2.1.3. EKO recalibration and extrapolation

As mentioned in section 1.5, in the previous thesis, W.Meines recommends that by recalibrating the EKO and albedometer device, the reconstruction errors may fall into acceptable ranges.

The EKO spectroradiometer is a measurement device which provides the user with measurements of spectral irradiance in the range of 300nm to 1150nm. In July of 2022, one of the EKO devices was sent to Japan for recalibration. Upon it's return in the beginning of September, the PVMD department was provided with the old, and new updated calibration function which could be applied to the EKO device.

Figure 2.3 shows the uncalibrated and calibrated EKO data on the 22nd September at 2pm. Observing the raw data, depicted as the red line, a large peak can be seen in the 1050nm range as well as an inverted peak around the 500nm wavelength. It can therefore be seen that the new calibration has not been applied and that the old calibration function was still in use. These anomalies in the raw data can be observed from the beginning of September to the 10th October. All the data in this time range therefore needed to be recalibrated by removing the old calibration and reapplying the new one, see the blue line in figure 2.3. In all the EKO data collected after the 10th October, the correct calibration is already applied.

After applying the new calibration, the spectrum is cut off at 350nm and 1050nm. According to the contact at EKO Instruments, this is due to an issue in the sensors measuring the extreme values of the spectrum which were therefore removed. The hardware of the albedometer device however, measures in the full wavelength range of 320nm to 1100nm which can not be changed without physical change to the device. It was therefore decided to linearly extrapolate the values of the EKO device in the ranges of 320nm to 350nm and 1050nm to 1100nm. The result of the extrapolation is shown in figure 2.4, where the red line is the recalibrated spectrum, and the blue points indicate the 20 points which were used to calculate the line of best fit and at the end of the red line, the linear extrapolation.

This extrapolation is applied to each of the EKO device measurements which are later used as a reference for error analysis. It is important to note that the extrapolated ranges can contribute to a slight inaccuracy in the error calculation; particularly in the end extrapolation where the spectrum is expected to tend downwards where water vapor in the atmosphere absorbs the wavelengths of light between 1070nm and 1220nm [32]. The effect of this can be seen in the SMARTS reconstructions in the results section, section 3.1, under figure 3.1, where the the tail of the reconstruction after 1050nm is expected to be lower than that of the reference spectrum.

2.2. Albedometer Calibration

2.2.1. Albedometer Calibration based on EKO reference device

The calibration of the albedometer was performed according to ISO 9847, Calibration of field pyranometers, [14]. The EKO device is used as the reference device. To complete the calibration, stable cloudless sky conditions, with the sun at elevation > 20°are required. Instantaneous voltage readings must then be taken "for a minimum of fifteen 10min to 20min measurement series, each consisting of 21 or more instantaneous readings" and must be taken over a 2 day to 3 day period. Using the CloudModel data, the days in table 2.2 were calculated as having the most stable and cloudless sky conditions by calculating the average SkyClass of each day in September:

Table 2.2: Clearest days in September according to CloudModel data.

Day	Average Clear Sky Index, K_c	Average Cloud Cover	Average SkyClass
22nd September 2022	0.9768	0	1.0252
29th September 2022	1.0396	0	1.0252
12th September 2022	0.9494	0.0014	1.1379

As previously mentioned in section 1.3. the albedometer has three upward facing sensors which must be calibrated. Figure 2.5 shows the range that each sensor measures. The red line is the spectral irradiance measured by the EKO device. Integrating the EKO spectrum over each sensor range, the

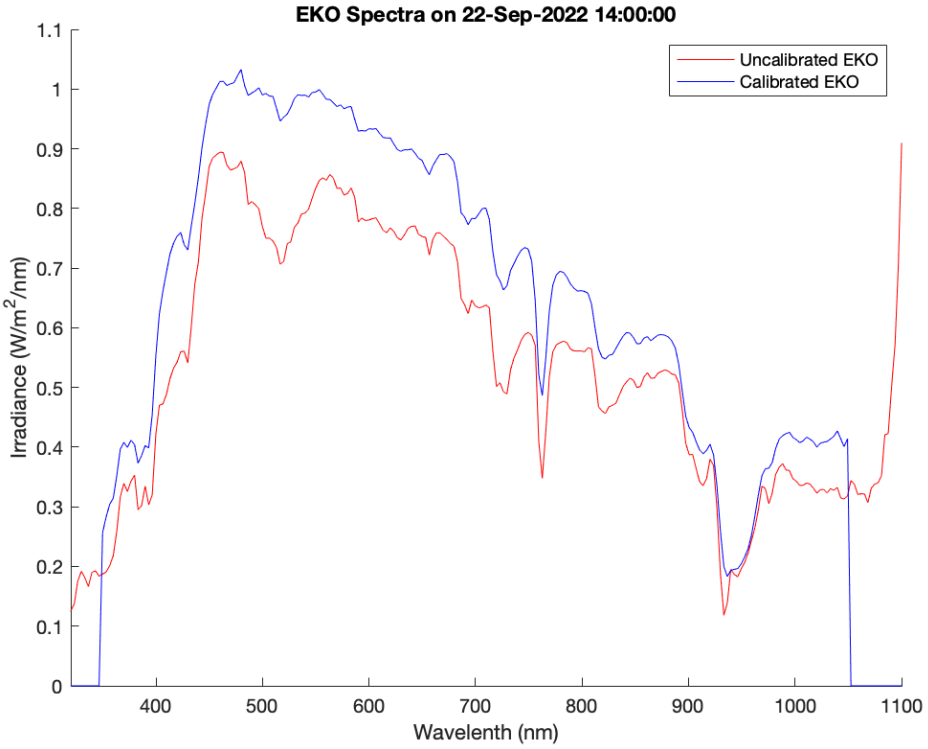

Figure 2.3: EKO data, before and after recalibration

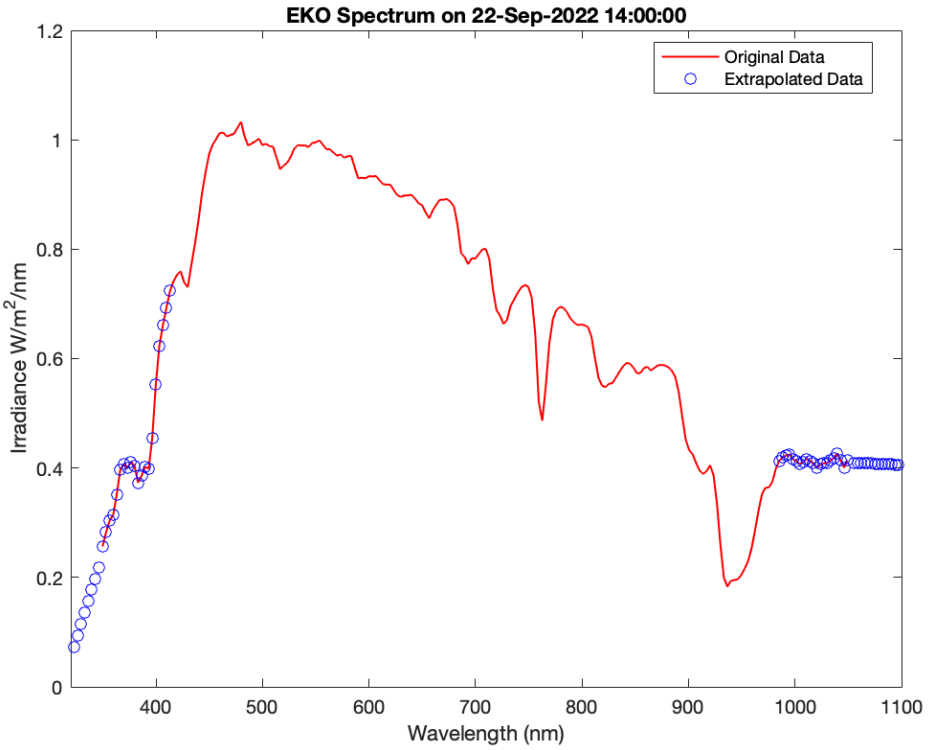

Figure 2.4: Linear Extrapolated EKO data between 320-350nm and 1050-1100nm.

'true' values of the irradiance in each sensor wavelength range are calculated. These values are then comparedto the measured albedometer sensor values; dividing the true value by the measured value, the calibration factor is calculated for each measurement. In order to meet the ISO 9847 requirements however, the EKO sensor integration must be repeated for each of the stable cloudless times for each day in table 2.2. A MATLAB code was written to extract all the albedometer sensor measurements and EKO spectra at times where SkyClass was equal to 1.

Dividing each albedometer measured value by its 'true' value, the calibration factor for each wavelength range is found, see table 2.3.

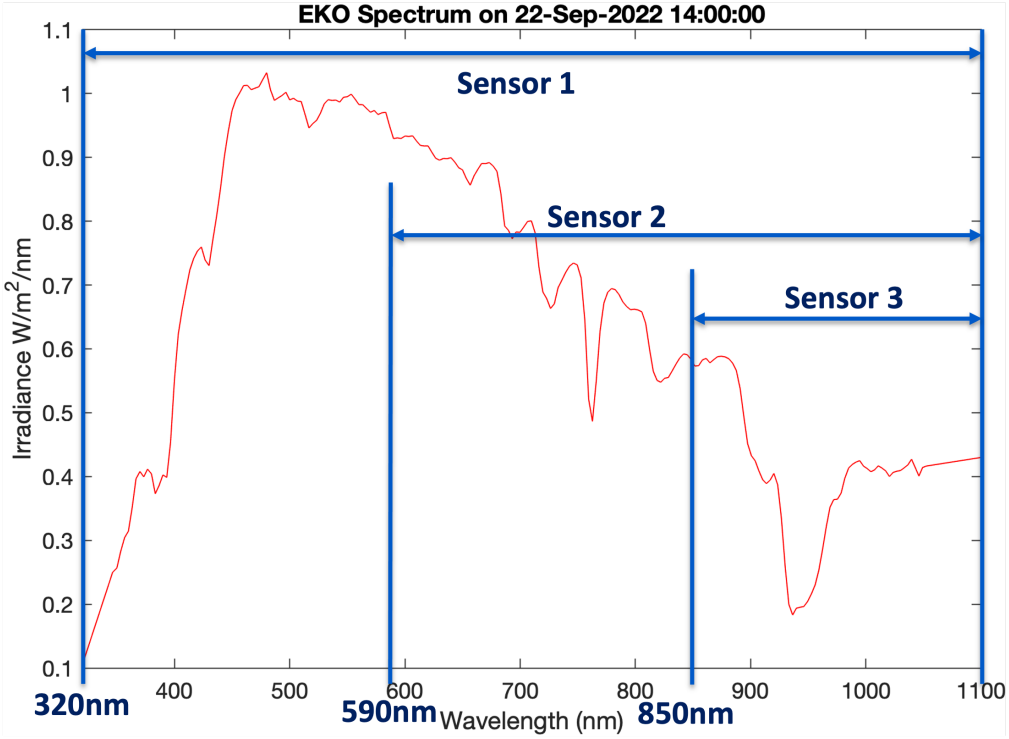

Figure 2.5: Measured albedometer sensor ranges against an EKO spectrum

Table 2.3: Calibration factors for each albedometer sensor.

Sensor Number	Sensor 1	Sensor 2	Sensor 3
Wavelength range (nm)	320-1100	590-1100	850-1100
Calibration Factor	1.5835	1.2792	0.7855

2.2.2. Calibration Validation

In order to validate the calibration, the calibration factors are applied to the sensors for clear-sky times outside of the times used for calibration. The results of the validation can be seen in figure 2.6. A slight cosine curve can be seen in the data with its lowest points at the edges around 9:30 and 18:00 and its highest point around 14:00. This curve is typical of a pyranometer's cosine response or 'directional response' and is related to the cosine response of the diffuser. The optimal diffusion within the device, and therefore, most accurate irradiance measurement, is when the sun is at its minimum zenith angle (maximum elevation) [4]. As the sun elevation decreases, the diffusion becomes less optimal within the device and the sensors measure less accurately.

The two spikes in relative error 3:02pm and 3:53pm come from an error in the sky classification code where cloudy sky conditions are incorrectly categorised as skyclass 1, see section 2.2.2, where the

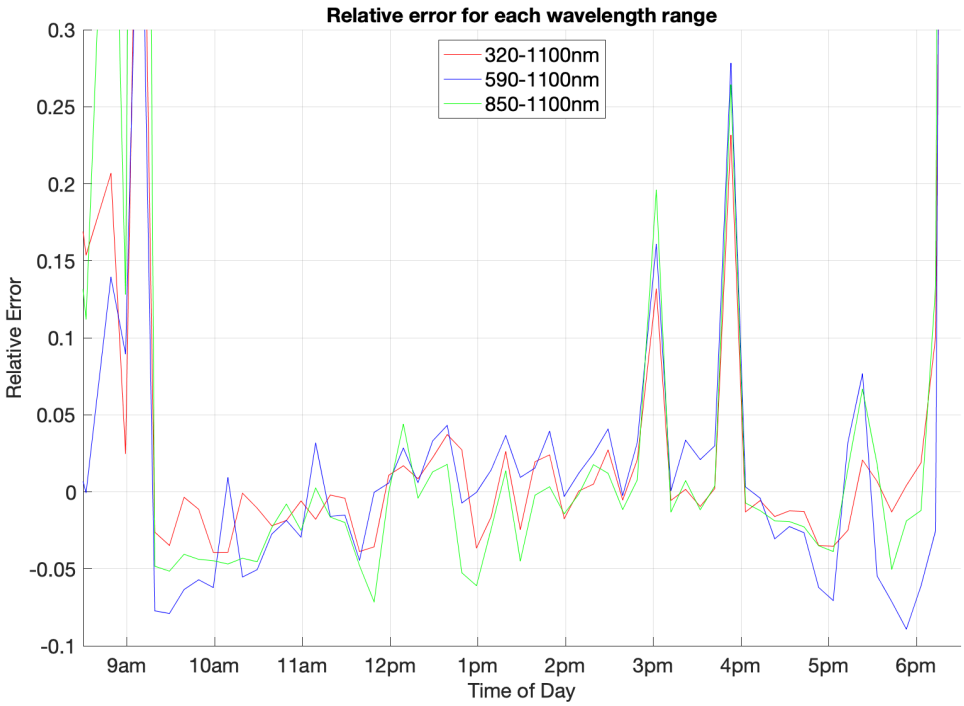

Figure 2.6: Calibration validation applied to times in September where SkyClass = 1.

sky image at 3:53pm on the 10th September 2022, is compared to the correctly classified sky image at 11:59am, 30th September, 2022.

The standard for calibration of pyranometers requires that only times with sun elevation > 20°[14] be used for calibration. In September, the month of data used to calibrate the device, 20°elevation occurs at approximately 9:45am and 17:30pm.

The calibration fails completely at times before 9:30am and after 6pm. These are the approximate times at which the sun becomes visible to the device after sunrise and before sunset in September, the month for which calibration was performed. Outside these times, the small irradiance measurements measured by the EKO and albedometer sensors can lead to large relative errors.

2.3. Spectral Irradiance Resconstruction

2.3.1. Resconstruction Method

Now that the recalibration of the EKO and albedometer has been performed, the reconstruction of the top-side spectral reconstruction can be performed so that we may assess the relative error of reconstruction.

The code for spectral reconstruction was adapted by W. Meines in his 2022 thesis project [23]. The spectral reconstruction uses the SMARTS clear-sky model [7] with the three top-side irradiance measurements as inputs, as well as three atmospheric parameters, computed using a PSO algorithm. More information on the model can be found in section 1.4.

The MATLAB class file 'PVMDalbedometer.m' is used, which contains the parameters and methods required to run the reconstructions. Such parameters include: the location coordinates, time zone, predominant albedo around 10km of the site, temperature coefficients and calibration factors. When the object is created from the class file, default values for the albedometer in Delft, are assigned to

(a) Sky image taken on 10th September 2022 at 15:53pm. Clouds surround and partly obscure the sun. Incorrectly classified as Skyclass 1.

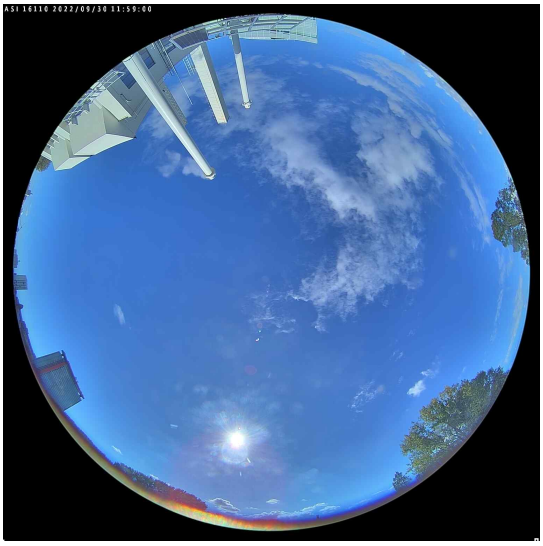

(b) Sky image taken on 10th September 2022 at 11:59am. Clear sky with few clouds present and away from the sun. Correctly classified as Skyclass 1.

the each of the parameters. The main method[1] in the 'PVMDalbedometer.m' class is used to run the SMARTS reconstruction and requires an array with the the calibrated values of measured irradiance in four wavelength bands: 320-1100nm, 320-590nm, 590-850nm, 850nm-1100nm.

The original class file, would require the user to manually extract, calibrate and split the sensor readings into their corresponding wavelength bands. To simplify this process, an additional method was added to the class file:

[albSensorValues, GHI] = calibrateSensorsGetGHI(obj, Time, albFile)

With inputs:

- **obj:** The object, and associated parameters such as Temperature coefficients and Calibration factors which are used for the calibration of the measurements.
- **Time:** Date and time the user would like to reconstruct in 'datetime' format.
- **albFile:** The file-path of the raw albedometer data file which contains the measurements at the desired date and time.

With outputs:

- **albSensorValues:** Array of calibrated values of measured irradiance in original sensor ranges, see table 1.1, for both the top and bottom sensors of the albedometer.
- **GHI:** Array of calibrated values of measured irradiance in the wavelength bands, see table 1.2, at the top of the device.

The 'GHI' output is used for top-side spectral reconstruction whilst the albSensorValues output is required for the spectral albedo reconstruction, as will be outlined in section 2.4. All the methods added to the 'PVMDalbedometer.m' class can be found in full, in appendix B.

To perform error analysis on the spectral reconstructions, the reference spectra from the EKO device are extracted for the same datapoints. CloudModel data is also collected so that the errors can be categorised by sky condition. Using the updated 'PVMDalbedometer.m' class method, a code is written which runs reconstructions continually.

914 Spectra were reconstructed, as visualised in figure 2.8.

[1] A method is a function which belongs to an object.

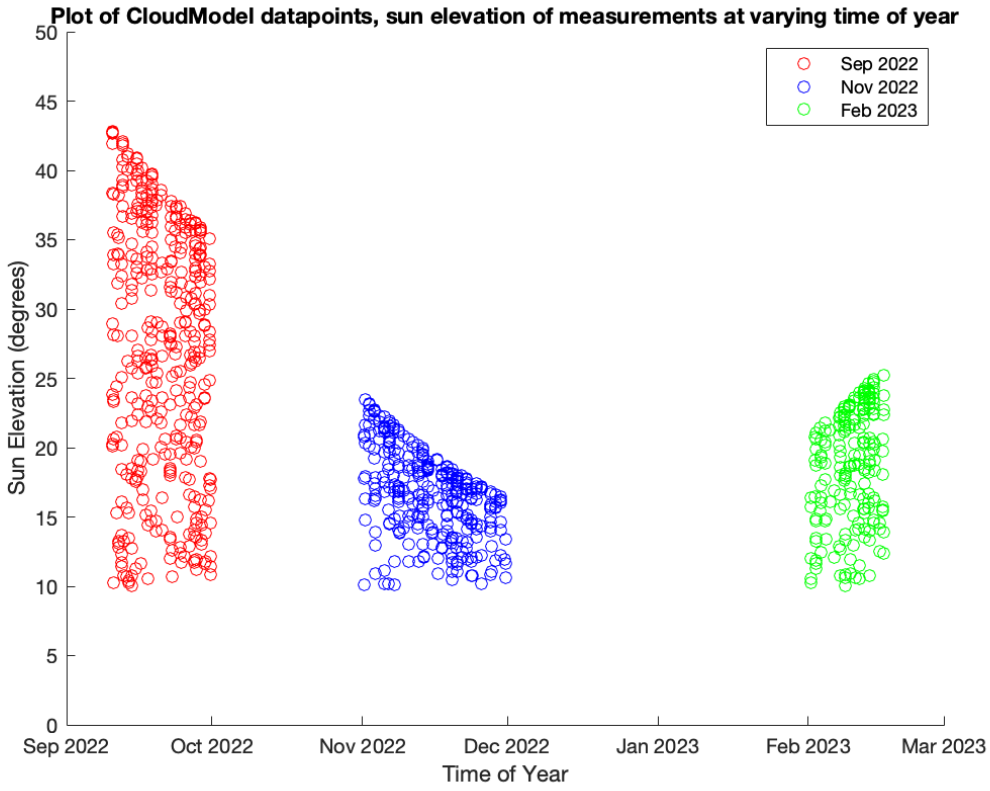

Figure 2.8: Dates of all 914 reconstructed spectra and their sun elevations.

2.3.2. Trace gas and Aerosol transmittance Investigation

The second recommendation from the previous thesis is to investigate how the Trace Gas and Aerosol Transmittance values can be optimised to reduce the error in the first wavelength range of 320-700nm where their concentrations most affect the spectrum [23].

According to the SMARTS manual [8], used for the spectral irradiance reconstructions, trace gas concentration can be changed using the parameter for tropospheric pollution (ILOAD), which varies from 1 - Pristine Atmostpheric Conditions, to 4 - Severe Pollution and Aerosol transmittance by changing the parameters of the Aerosol model below. The default values from the S&F Rural Aerosol Model in SMARTS [30] are also indicated:

- ALPHA1 - Average value of Ångström's wavelength exponent α for wavelengths < 500nm (generally between 0.0 and 2.6). Default value = 0.999.
- ALPHA2 - Average value of Ångström's wavelength exponent α for wavelengths > 500nm (generally between 0.0 and 2.6). Default value = 1.5650.
- OMEGL - Aerosol single scattering albedo (generally between 0.6 and 1.0). Default value = 0.94.
- GG - Aerosol asymmetry parameter (generally between 0.5 and 0.9). Default value = 0.67.

A code is therefore written which runs a reconstruction for every possible combination of ILOAD, and for each of the Aerosol model parameters at their minimum, maximum and median value. Reconstructions were performed in the wavelength ranges 320-590nm, as recommended by the previous thesis, and where the effects of the parameters most affect the spectrum [23]. Analysing the errors of each reconstruction should give an idea as to which combination is best for the reconstruction in the first wavelength band.

2.4. Spectral Albedo Reconstruction

Spectral albedo is a complex measure of irradiation energy based on many environmental factors, as described in, section 1.2. In H. Ziar's 2019 paper on spectral albedo modelling, the equation for spectral albedo, equation (1.1), is a function of the spectral reflectivity and roughness of the ground, the view factor of shaded and unshaded parts of the ground, the solar position and sky conditions [36]. At this point in the project, the albedometer is capable of providing the reconstructed spectral irradiance and the measured albedo from to the sensors at the front and back of the device. The purpose of this topic of investigation, is to reconstruct the multi-dimensional equation of spectral albedo using the limited information measured by the albedometer sensors, as well as the information which can be provided by the user.

In order to predict spectral albedo using the available inputs, it was decided to use a Machine learning (ML) model. Machine learning is a branch of artificial intelligence (AI) and computer science which imitates the way that humans learn by analysing the patterns and relationships between its inputs (features) and target output(s) [10].

In this case, the target output is an array of spectral albedo values, with one value per wavelength increment. At the beginning of this thesis, it was planned that the spectral albedo could be measured using two EKO devices arranged back to back alongside albedometer. This data would have also served to calibrate the down facing sensors of the albedometer. However, due to a delay in the supply of the support structure, the devices could not be installed in time. The calibration of the down facing sensors was therefore assumed to be the same as those of the corresponding top-facing sensor. Since the real values of the target spectral albedo, $\alpha(\lambda)$ could not be measured using the two EKO devices back to back, a simplified spectral albedo can instead be calculated as such:

$$\alpha(\lambda) = \frac{G^{down}(\lambda)}{G^{up}(\lambda)} \tag{2.1}$$

Where G^{down} and G^{up} are the measured irradiance at the bottom (down facing) and top (up-facing) of the device. G^{down} can then be approximated as:

$$G^{down} = r(\lambda) \cdot G^{up} \tag{2.2}$$

Where G^{up} is the measured irradiance by the EKO spectroradiometer. Therefore, the simplified spectral albedo equation is:

$$\alpha(\lambda) = \frac{r(\lambda) \cdot G^{up}(\lambda)}{G^{up}(\lambda)} \tag{2.3}$$

In equation (2.3), $r(\lambda)$ is the spectral reflectance of the material as a percentage (the effectiveness of reflecting radiant energy at different wavelengths) and is gathered from the ASTER spectral library [2]. A 'Gray/dark brown extremely stoney coarse sandy' material was chosen as the closest to the pebble material under the albedometer. The sample reflectance data in the model's wavelength range can be found in appendix A.

As the G^{up} components in equation (2.3) are the same, the equation for spectral albedo becomes $\alpha(\lambda) = r(\lambda)$. As the model inputs already include the reflectivity $r(\lambda)$, a machine learning model would not provide significant benefit in this instance. A modified model was designed which predicted the spectral albedo without the reflection spectrum as an input, these results would demonstrate whether the reflectance spectrum was necessary for the reconstruction. However since the output was constant and equal to the reflectivity spectrum of the ground material, the model became over trained and could reconstruct the spectrum irrespective of the values of the model's features. The results of this model are shown in section 3.2.

To demonstrate the potential for ML models in spectral albedo reconstruction the target output was changed to that of the down-facing spectral irradiance (DFSI), described in equation (2.2). Since the $r(\lambda)$ and G^{up} are both components of both spectral irradiance and DFSI, the complexities of spectral albedo, which vary with time, sky condition and ground reflectivity, can be captured and predicted by

the ML model for DFSI reconstruction. The predictions from this ML model will demonstrate the potential effectiveness of this reconstruction method when the real spectral albedo values can be measured in situ using the EKO devices.

Table 2.4 indicates the chosen features and target output for this model. The features provided to the model were chosen as being most relevant to the spectral albedo reconstruction. Sun elevation was also added due to its observed effects in the results of the top-side spectral reconstruction, see section 3.1.2, but also due to its reported effect on spectral albedo in literature [20].

Table 2.4: List of all the features (inputs) and target output used to train the machine learning model.

Features	
Wavelengths:	Wavelength array from 320-1100nm with same intervals as SMARTS reconstruction.
Top sensor values	Measured irradiance at the top of the device in wavelength bands 320-590nm, 590-850nm and 850-1100nm.
Bottom sensor values:	Measured irradiance at the bottom of the device in wavelength bands 320-590nm, 590-850nm and 850-1100nm.
Sensor albedo values:	Bottom sensor values divided by top sensor values.
SMARTS reconstruction:	Spectral irradiance reconstruction values from SMARTS model.
Material spectral reflectance:	Material reflectance for the complete wavelength range.
Sun elevation:	Sun elevation at the time of measurement.
Target Output	
Rear-side spectral irradiance:	Rear-side spectral irradiance calculated by multiplying the material reflectivity and EKO top-side irradiance spectrum, equation (2.2).

Two machine learning models were investigated: Gaussian Process Regression (GPR) and Random Forest (RF) modelling. GPR modelling was originally chosen for its ability to model complex patterns and the ability to provide probabilistic outputs. Such outputs can provide the user with the uncertainty at each point in the reconstruction and can help to inform which features most benefit the model [34]. However, GPR is not a very scalable model, and failed to analyse the large dataset as the number of instances grew. Random Forest Modelling is highly scalable and also able to capture complex non-linear relationships within the data [12].

When training a machine learning algorithm, one main risk is overfitting the data [11]. Overfitting means that the model becomes overly well trained on the training data, and does not accurately predict unseen data. This is often caused by high model complexity. To prevent and detect overfitting in the machine learning model, 70% of the data was used for training and the remaining 30% used for testing. By splitting the data, it's possible to analyse the error of reconstructions on data which is completely unseen by the training model. Random Forest modelling is an 'Ensemble method', meaning that the model chooses the most popular output from many decision tree classifiers. It's possible to increase the number of decision trees used for training the model, thereby increasing the complexity of the model. As the complexity increases, so is the likelihood of overfitting. To determine the number of trees which should be used for modelling, the mean squared error (MSE) of the models is calculated for increasing number of decision trees, see figure 2.9. It should be noted, that the mean squared error is mostly useful in comparing different machine learning parameters such as the number of trees, rather than as an intuitive measure of error. The MSE can be seen to decrease at first, then begins to plateau after 120 decision trees. The model was chosen therefore to be trained with 120 decision trees, as to prevent overfitting by overtraining.

The size of the dataset, the number of total 'instances' collected for each parameter was 768,954. These instances are composed of 861 wavelength increments between 320 and 1100nm meaning that 914 total spectra were collected for modelling. The total collected data was then split into unique Sky-class categories and separate models were trained for each, see table 2.5 to investigate how the sky conditions would affect the accuracy of the down-side spectral irradiance reconstructions.

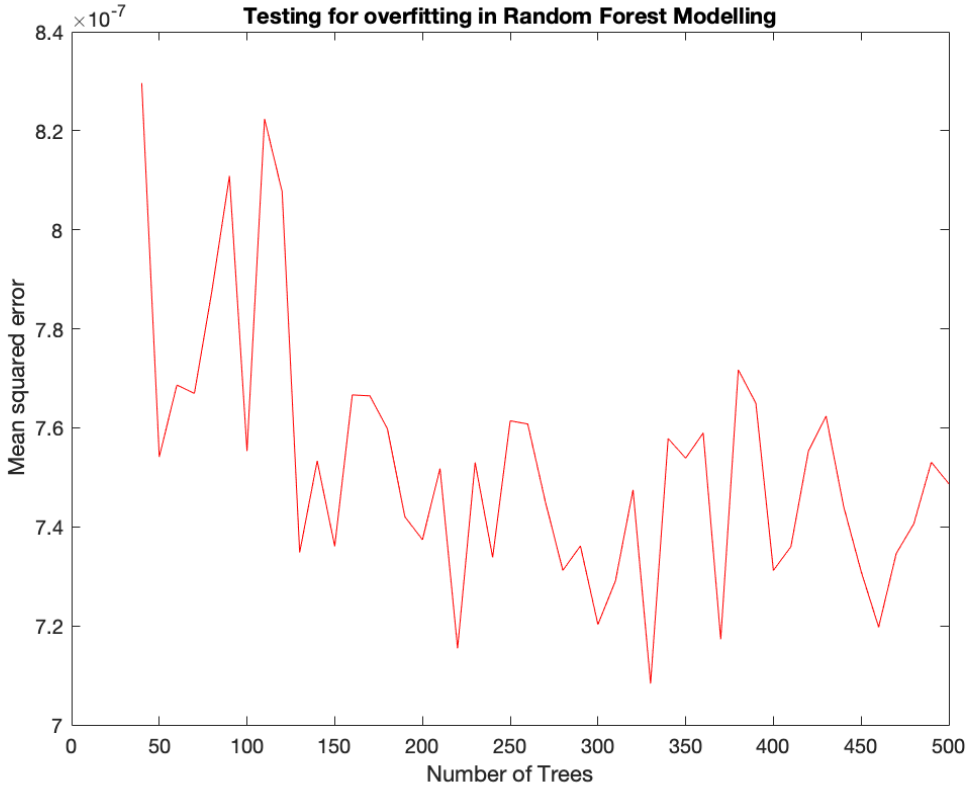

Figure 2.9: Mean Squared Error of random forest model reconstructions with increasing number of trees (model complexity).

Table 2.5: Size of each Random Forest model dataset for training and testing.

Skyclass	Num. spectra	Num. instances
All	914	786,954
1	289	248,829
2	114	98,154
3	67	57,687
4	307	264,327
5	137	117,957

2.5. Albedometer App

As demonstrated in section 2.3 and section 2.4, running the spectral reconstructions requires in depth knowledge of the MATLAB coding language which the average user may not have. Furthermore, preparing the required inputs for the reconstructions can be time-consuming. The purpose of the Albedometer app is to improve the usability of the albedometer device by designing an app capable of running both the top-side spectral irradiance and spectral albedo reconstructions in an intuitive manner, thereby reducing the amount of time spent between measured input and reconstructed output.

First, according to the possible use cases of the device investigated in the literature review, section 1.1, a list was made of the target end-users, outlined below. The end users are assumed to be technically knowledgeable in the installation and operation of measurement instruments.

PV systems designers, owners and operators:

- Measuring daily & seasonal variation of irradiance and spectral albedo for determining suitable location for PV farm construction
- Energy yield prediction pre-installation
- Performance tracking of PV installation - remote sensing of spectral irradiance and spectral albedo

Urban planners and material scientists:

- Spectral albedo tracking due to urbanisation effects
- Pre- and post- construction effect on measured spectral albedo
- Spectral albedo measurements of materials for Urban Heat Island reduction

Wildlife conservationists:

- Analysing quality of snow and ice in polar regions
- Remote sensing of seasonal fluctuations of ice sheets and snow.

Based on the target users which may interact with the device and the required inputs of the device, thee following design requirements were chosen:

- Intuitive to navigate and well labeled
- Minimize user inputs
- Process and prepare raw albedometer files for reconstruction
- Perform reconstruction of spectral irradiance and spectral albedo
- Visually display reconstructions
- Export reconstructed data to .csv datafile
- Operate without internet connection

As the spectral irradiance and albedo reconstructions were performed in MATLAB, the app was designed in MATLAB App Designer and requires the following inputs:

- Raw albedometer file in .csv format (see appendix A
- Date and time of desired reconstruction
- Ground material type
- Sky conditions at selected date and time
- Longitude and latitude at albedometer location
- Altitude of the albedometer

3

Results and Discussion

3.1. Spectral Irradiance Reconstruction

In this section, results of spectral irradiance reconstructions are outlined and discussed. The aim of this section is to demonstrate how the recalibration of the albedometer device and trace gas and aerosol transmittance investigation can improve the error of the spectral irradiance reconstructions, thereby answering the first research question:

Can the recalibration of the albedometer improve the error measurements of the device or is a physical change to the device required?

The results of the following subsections will answer the recommendations from the previous thesis [23]:

1. Repeat error analysis with recalibrated EKO and albedometer.
2. Aerosol transmittance and trace gas investigation.
3. Place additional sensors.

3.1.1. Error analysis with recalibrated device

In this section, the results of the spectral irradiance reconstructions, with the recalibrated albedometer device, are shown. Spectral irradiance reconstructions are performed for 914 spectra. For each reconstruction, the reference spectrum is extracted from the EKO device measurements and the sky classification data is collected to determine the sky condition at the reconstruction time.

Figure 3.1 shows two sample reconstructions compared to their reference EKO spectra at the same time. Despite using the same reconstruction method, both of the spectra have visible differences, notably around 950nm where in some reconstructions, the dip at 950nm is not simulated. Where this dip is not present however, the accuracy of reconstructions is improved in the wavelengths before 700nm and vice-versa. This phenomenon also present in the the previous thesis [23], is due to the estimation of Aerosol optimal depth, Ozone reduced path-length and total precipitable water estimated using the PSO algorithm, previously discussed in section 2.3. The algorithm, which attempts to minimise the error in each of the sensors' wavelength ranges prioritises either the value of total precipitable water, which affects absorption periodically after 700nm, or those of Aerosol optical depth at 550nm and Ozone reduced path-length between 320-350nm and 450-750nm [23].

Additionally, as mentioned in the methodology for the EKO recalibration, section 2.1.3, there is a visible mismatch in the tail of the reconstruction after 950nm where the spectrum of the EKO device is linear extrapolated where the recalibrated spectrum was cut-off.

In the previous thesis, a results table is shown, indicating the relative errors of the irradiance reconstruction model in each wavelength band for clear-sky conditions (Skyclass = 1) and GHI > 400. The relative error of these 99 reconstructed spectra which meet these same conditions are visualised in

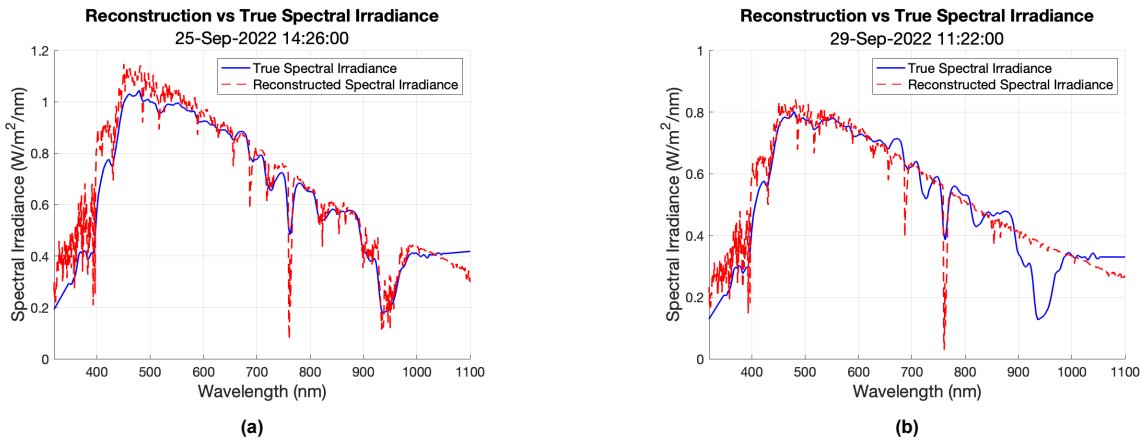

Figure 3.1: Two sample clear-sky reconstructions of spectral irradiance compared to the reference spectrum measured by the EKO device. Figure 3.1a is for the condition where total precipitable water is correctly found, and figure 3.1b is for when Aerosol optical depth and Ozone reduced path-length parameters are correctly found.

figure 3.2. Each spectrum is coloured differently and sorted by increasing colour 'height' according to the GHI of the reconstruction. The errors in each wavelength band, as compared to those measured before the new device calibration, can be found in table 3.1. The results, compared to the wavelength bands and uncertainties of the EKO device, are shown in table 3.2.

Table 3.1: Relative errors of spectral reconstructions measured in the previous thesis [23] compared to reconstructed values with a recalibrated device. The 'Range' rows indicate the range of the 95% confidence interval.

		Wavelength range [nm]			
		320-590	590-850	850-1100	Total (320-1100)
Relative error Old Calib. [%]	Range	[11.3, 9.1]	[-2.1, 4.9]	[-4.6, 10.1]	[-6.2, 8.2]
	Mean	-1.9	2.1	2.3	0.82
Relative error New Calib. [%]	Range	[3.49, 7.23]	[-5.44,-2.81]	[0.75,4.62]	[-0.78, 2.13]
	Mean	5.36	-4.12	2.69	0.67

Table 3.2: Reconstruction errors before and after new calibration vs EKO reported uncertainties [23]. The 'Range' rows indicate the range of the 95% confidence interval.

		Wavelength range [nm]		
		350-450	450-900	900-1050
Before new Calibration	95% error range [%]	[-11.62, 11.87]	[-3.92, 3.73]	[-3.3, 12.75]
	Mean error [%]	-1.43	0.43	4.07
With new Calibration	95% error range [%]	[13.2,18.48]	[-4.3, -1.48]	[8.35, 13.79]
	Mean error [%]	15.84	-2.89	11.07
EKO uncertainty [%]		$\pm$ 11.35	$\pm$ 5.00	$\pm$ 4.39

Three clear error fluctuations can be observed in figure 3.2. Between 320 and 400nm, the the relative error is noticeably large, though due to the low values of irradiance in this range, the error can appear exaggeratedly large. Such is the case also for the wavelength range 900-1000nm where the atmospheric absorption due to water vapour occurs. The reference value of irradiance can drop below 0.2 W/m^2/nm, meaning that in the case that the 'total precipitable water' dip is not correctly reconstructed, as demonstrated in figure 3.1b a large relative error can be calculated even though the absolute error may not be as large as the absolute error at 770nm for instance. At 770nm, there is am error fluctuation due to trace gas transmittance, an atmospheric parameter used in the SMARTS program.

The results in table 3.1 show how the range of the reconstructions errors have improved in each wavelength band as compared to the in the previous thesis. In each of the wavelength bands, the range

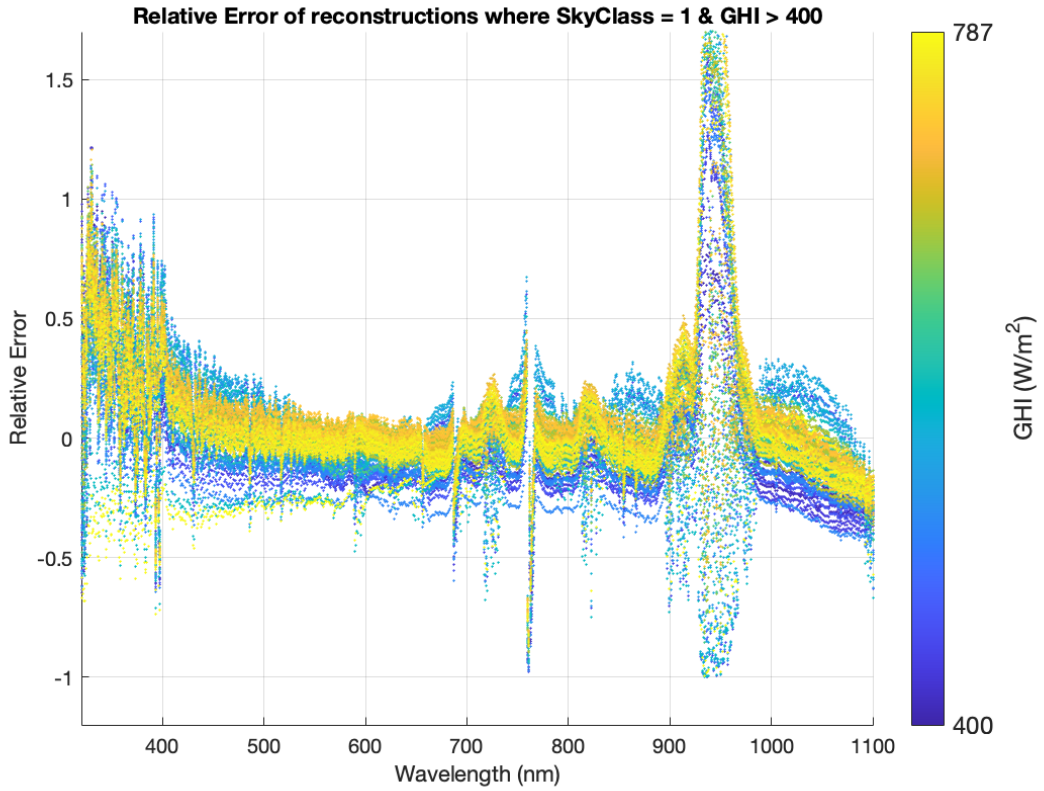

Figure 3.2: Relative Error of all 99 reconstructions which have a Skyclass of 1 and GHI above 400. Each spectrum is plotted in a different colour and the increasing 'height' of the colour, indicated by the colour bar on the right, corresponds to increasing GHI value.

95% confidence interval has decreased significantly, however, the mean values have shifted further from 0 than in the previous thesis, as will be discussed in section 3.1.4. The results in table 3.2 show that with the new calibration, only the central wavelength bound stays within acceptable bounds. For the remaining reconstruction ranges, whilst the error ranges have decreased, the mean error of reconstructions overestimates the correct values, though as previously mentioned, due to the low values of irradiance in the 350-450nm and 900-1050nm ranges, the relative error can appear much larger than its absolute values. These two wavelength ranges also coincide with the regions in which the atmospheric parameters of trace gas transmittance, ozone transmittance and water vapor are most affecting the spectrum.

3.1.2. Reconstruction Error in Changing Sky Conditions

In this section, the results of the reconstructions will be plotted for changing conditions: sun elevation, GHI, Skyclass, Cloud cover and Clear sky index.

The relative error of all reconstructions with increasing sun elevation and GHI can be found in figure 3.3. The figures show that with increasing GHI or sun elevation, the relative reconstruction error decreases in each wavelength band. The SMARTS irradiance reconstruction model is designed for clear sky conditions. High GHI measurements will only occur in clear sky conditions when the sun is unobscured, therefore decreasing the reconstruction error with increasing GHI. In high sun elevation times figure 3.3a, a higher GHI is expected due to the decreased angle of incidence between the sun and the device and therefore lower error. However, high sun elevation does not guarantee that clear-sky conditions are present, hence the large number of random outliers in figure 3.3a where non-clear sky conditions are present.

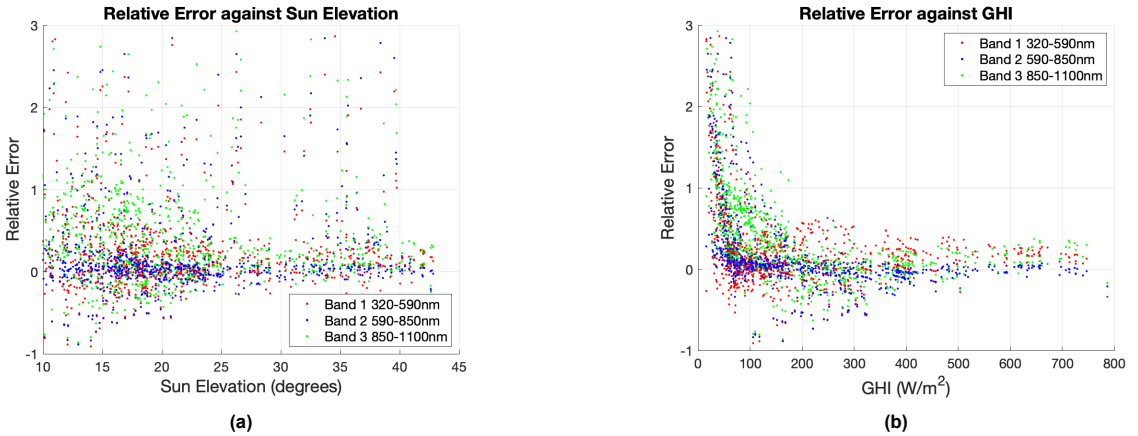

Figure 3.3: Relative Error of reconstructions in each wavelength band, with changing sun elevation and GHI at the time of measurement.

To understand which sky conditions lead to the most accurate results, the accuracy of the reconstructions is compared to the Skyclass at the time of measurement, see figure 3.4. Skyclass 1, 2 and 3, representing clear-sky, partly cloudy and overcast with high irradiance are the three categories with highest accuracy. Skyclasses 4 abd 5 have significantly lower reconstruction accuracy. The high accuracy of the overcast skyClass 3, even relative to Skyclass 2, is surprising given that SMARTS is only for use in clear-sky conditions. Referring again to figure 2.1 in section 2.1.1, Skyclass 1, 2 and 3 each have high Clear Sky Index (K_c) in common, indicating that accuracy of reconstruction may overcome high cloud cover if the clear sky index is sufficiently high. Figure 3.5 shows how reconstruction error decreases with decreasing cloudcover and increasing clear sky index. It is possible, given this data, to determine the minimum or maximum values of these sky conditions which returns an accurate reconstruction.

3.1.3. Trace Gas and Aerosol Transmittance

As explained in section 2.3.2, the trace gas and aerosol transmittance values are atmospheric parameters which affect the absorption of light in different wavelength bands. Trace gas levels in the SMARTS reconstruction method are changed by varying the value for 'tropospheric pollution' (ILOAD). Aerosol transmittance is changed by changing the values of Ångström's wavelength exponent, before and after 500nm (ALPHA1, ALPHA2 respectively), Aerosol single scattering albedo (OMEGL) and Aerosol asymmetry (GG). Each of these values have a range of 'normal' values, and the method for this analysis is to reconstruct the spectrum for every combination of Trace gas and Aerosol Transmittance values.

Each of the Aerosol Transmittance parameters is tested at the minimum, median and maximum of its 'normal' range whilst the trace gas is tested for each value from 1 to 4 where 1 is the least pollution, and 4 is the most. Therefore, to perform this analysis, for one clear-sky measurement on the 14th February 2023 at 13:20, 324 reconstructions are performed. The results can be found in figure 3.6 where the absolute error is shown for every possible combination of Trace gas and Aerosol transmittance parameter. The graph also shows the normal value of the SMARTS reconstruction in band 1 when the parameters are kept as default in the red dotted line. The graph shows that the only parameter which significantly reduces the error of reconstructions is the tropospheric pollution parameter, ILOAD, indicated as the green circles in figure 3.6. The least error occurs when ILOAD = 4, this is equivalent to 'Severe Pollution', very unlikely for the city of Delft.

3.1.4. Discussion

The results shown in table 3.1, indicate that, relative to the results of the previous thesis, the recalibration of the albedometer has helped in reducing the range of errors in first and last wavelength bands, including the full wavelength range. The range of errors has increased slightly in the 590-850nm band. The mean values however, have shifted upwards in the first and last wavelength bands whilst the middle wavelength band has shifted downwards.

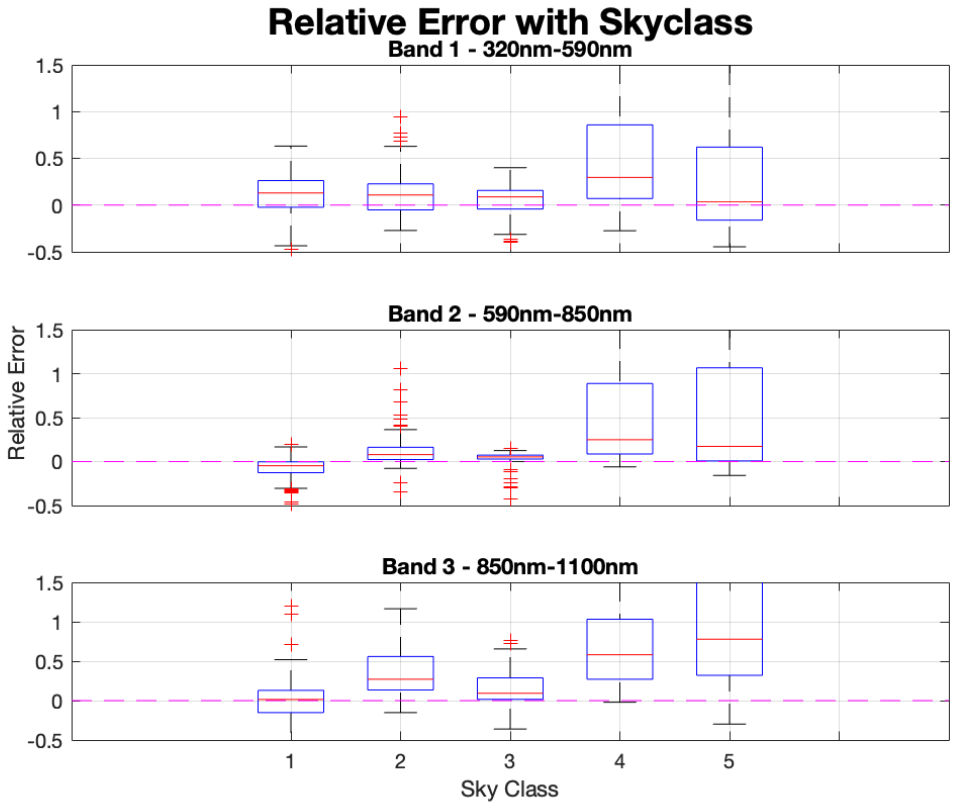

Figure 3.4: Relative Error of all reconstructions, split into Skyclass categories. Boxplots indicate median value, 25th and 75th percentiles, the range of data excluding outliers and the outlier points marked as red crosses.

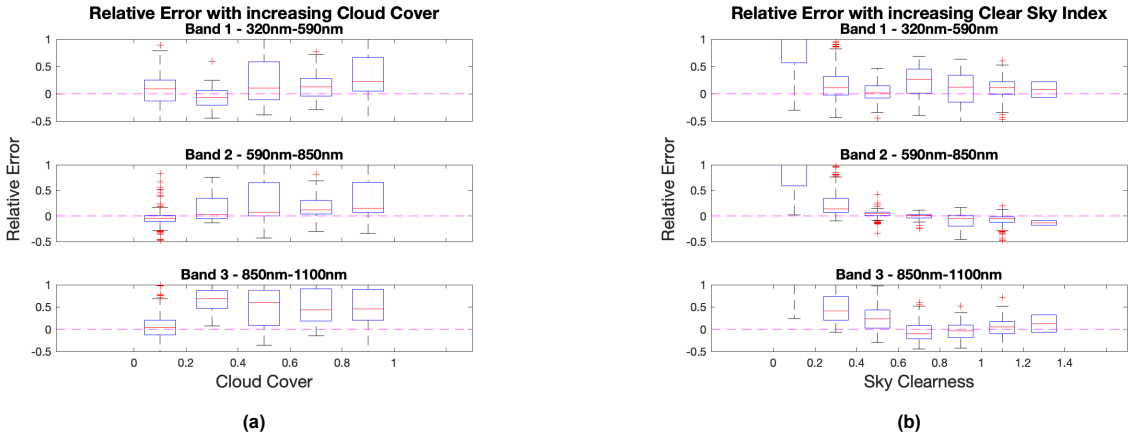

Figure 3.5: Boxplots of relative errors of reconstructions with changing Cloud Cover and Clear Sky Index respectively.

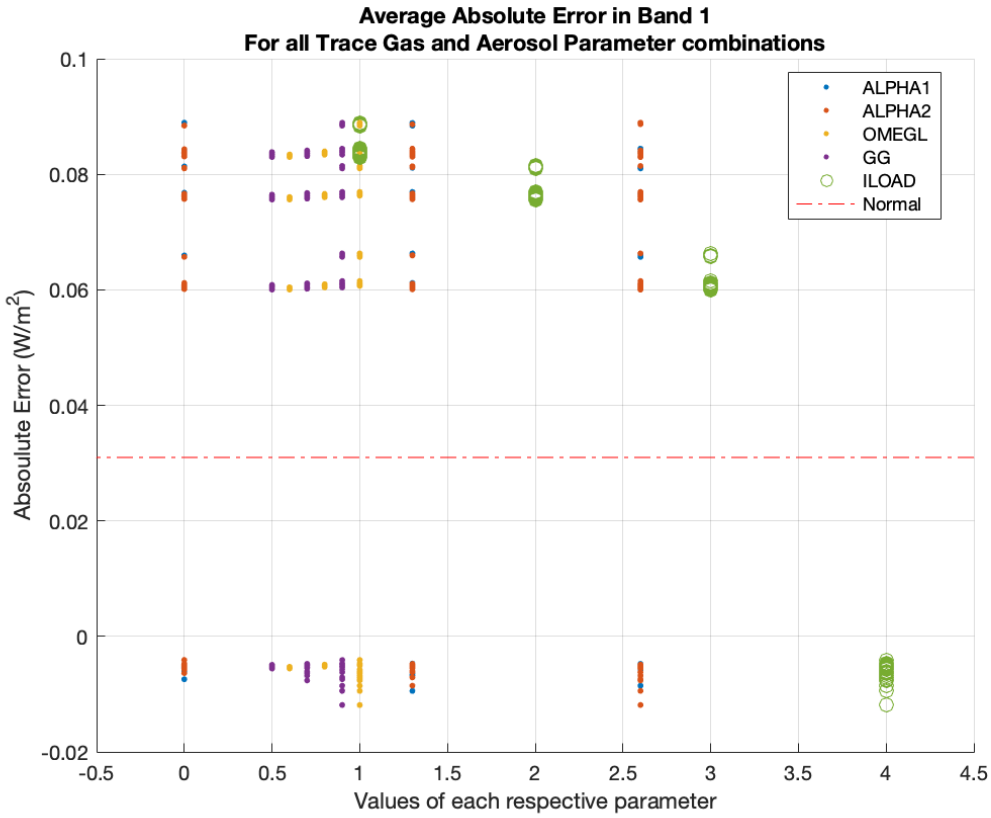

Figure 3.6: Plot showing the average absolute error in Band 1 (320-290nm) for every combination of Trace gas and Aerosol transmittance parameter in the SMARTS model. The x-axis indicates the value of each individual parameter

The reason for this shift may be tied to the results shown in table 3.2 in which significant shifts in the mean errors of the first and last EKO ranges can be observed whilst the error ranges have decreased. As explained in section 3.1.1, the first and last wavelength ranges, 350-450nm and 900-1050nm coincide with the regions in which the atmospheric parameters of Trace gas transmittance, ozone transmittance and water vapor are most affecting the spectrum. Improving the accuracy of these parameters may help to improve the model's mean error in these ranges. Specifically in the 900-1050nm range, the SMARTS model does not always reconstruct the dip, ususally caused by water vapor in the atmosphere, see figure 3.1b.

The ozone transmittance parameter 'Ozone reduced pathlength' and water vapor parameter 'Total precipitable water' are determined by the PSO algorithm, as explained in section 1.4. The previous thesis has shown that the algorithm can be improved by changing the weights of the PSO algorithm so that the parameters converge to more accurate values.

Therefore, to answer the first part of the first research question: the recalibration of the albedometer device from the recalibrated EKO device helped to reduce the range of errors, but the mean value of error lay outside of the required uncertainty bounds. Changing the weights of the PSO algorithm should help to remedy this shift by estimating more accurate values of the three atmospheric parameters. Furthermore, the algorithm should be adapted to ensure that the water vapor transmittance between 800-900nm is modelled consistently in every reconstruction.

Section 3.1.3 helps to answer the second part of the first research question. According to the results in figure 3.6, there exists no 'logical' combination of parameters which compose aerosol transmittance or trace gas transmittance which lead to a lower absolute error than the default conditions. The only

reconstruction which performed better was when the tropospheric pollution parameter 'ILOAD' was set to 'Severe Pollution', which is highly unlikely, given that default value of tropospheric pollution was of 'light pollution'.

The findings demonstrate that the aerosol parameters has little effect on the reconstructed error and that the trace gas parameter, whilst having a larger effect, does not make logical sense to change in this case. This analysis was completed for one specific clear-sky time. More comprehensive solutions could be drawn through repetition of the analysis for other date and time combinations, however this was not possible within the time constraints of the research.

Finally, based on these results, it must be decided whether an additional sensor should be installed to improve the error reconstruction in the first wavelength band. The first reconstruction analysis showed that the range of results was decreased significantly after the device was recalibrated, these reconstructions however, were shifted outside of acceptable bounds. The trace gas and aerosol transmittance investigation indicates that changing these parameters does not greatly effect the error, however the adjustment of the PSO algorithm may be able to shift the errors back to acceptable levels. In this case, an additional sensor is not required. The additional purpose of adjusting the PSO algorithm, is to correctly simulate the water vapor transmittance between 800-900nm. If this does not work, it may also be possible to install the sensor in the same range, helping to measure the value for water vapor transmission in the same was as the Spectrafy device [32].

The results of the error analysis based on changing sky conditions, section 3.1.2, were useful in helping to select relevant parameters for the spectral albedo reconstruction and sky-condition inputs for the Albedometer App. It was demonstrated that sun elevation and GHI has a noticeable effect on the reconstructions. Skyclasses 1, 2 and 3 are also the most accurate reconstructions and that low cloud cover and high Kc are desired for accurate reconstructions.

Based on these findings, it was decided to add the sun elevation, GHI and Skyclass as inputs for the machine learning model for the reconstruction of spectral albedo.

3.2. Spectral Albedo Reconstruction

In this section, two models are trained to demonstrate the potential for Machine Learning models in spectral albedo reconstruction, thereby answering the second research question:

Can a model be built to reconstruct spectral albedo using the data available to the device?

The results of the following subsections will demonstrate that spectral albedo prediction using forest model machine learning can be performed to a high accuracy and comments are outlined on which input parameters are most important for the reconstructions.

3.2.1. Spectral Albedo Results

The first model, aims to reconstruct the spectral albedo as calculated in equation (2.3) using the all the features listed in table 2.4 excluding the ground material spectral reflectance. Figure 3.7 shows one reconstruction of the spectral albedo, where the blue line is the real spectral albedo and the red dashed line is that of the spectral albedo reconstruction. The lines in figure 3.7 are almost overlapping and the relative error of the reconstruction is very low at less than 1% uncertainty in the entire wavelength range. This is a result of an over-trained model given that the spectral albedo is constant in every reconstruction, meaning that the model is reconstructed perfectly, irrespective of the values of the model's features.

3.2.2. Down-facing Spectral Irradiance Results

The model for down-facing spectral irradiance (DFSI) was first trained with only Skyclass 1 data. This is because the spectral irradiance reconstruction model is made to function in clear sky conditions and because the reconstruction accuracy in this range was highest according to section 3.1.2. Four exam-

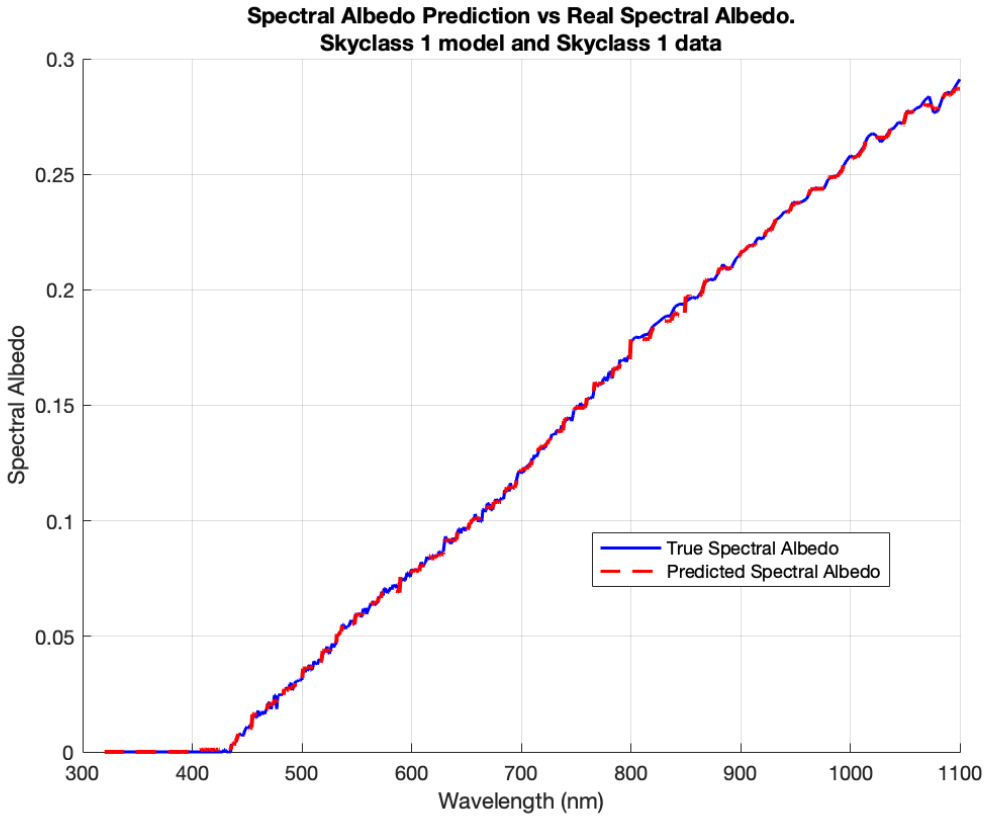

Figure 3.7: Reconstructed spectral albedo using machine learning model trained using Skyclass 1 data. Spectral albedo on the y-axis is unitless.

ple ranges of DFSI are shown in figure 3.8. The red dotted lines indicate the reconstructed (predicted) irradiance whilst the blue solid lines indicate the 'real' target irradiance calculated using equation (2.2).

The line of predicted irradiance in figure 3.8 approximates the target value well. The measured mean error and 95% confidence interval range of each band is shown in the first row of table 3.3. Following the successful reconstruction of the Skyclass 1 data, it was decided to test the Skyclass 1 model with Skyclass 2 data. As demonstrated in figure 3.9, the reconstruction fails completely, the mean reconstruction error in each band jumps to over 50% overestimation, showing that the model is extremely sensitive to the Skyclass of the data being used in the model. This is an important phenomenon, which needs to be addressed, as it is not possible for the user to know the exact Skyclass at a certain time without a sky camera at their disposal.

Additional models were trained with data from each one of the 5 Skyclasses. This way, depending on the sky conditions at the measurement time, the correct model can be used for reconstruction. The reconstruction error for each Skyclass model with corresponding Skyclass data can be found in table 3.3. The cited measurement uncertainty of the Spectrafy SolarSIM:Alb is 5% [31]. Comparing the reconstruction uncertainties of the TU Delft albedometer device to that of Spectrafy, Skyclass models 1 and 2 both pass with under 5% uncertainty in each of the wavelength bands.

As explained in section 2.4, the reflectance of the material under the albedometer is estimated and a sample reflectivity spectrum is used from the ASTER spectral library [2]. In reality, even if the material type is accurately guessed, the actual material reflectance will be slightly different. The sensitivity of the model with changing reflectivity is therefore analysed. For this analysis, the average value of the reflectivity spectrum is calculated (12%), then 1%, 10% and 20% of the average is added to each of the points in the reflectance spectrum. The resulting reconstruction error using SC 1 data in the SC 1

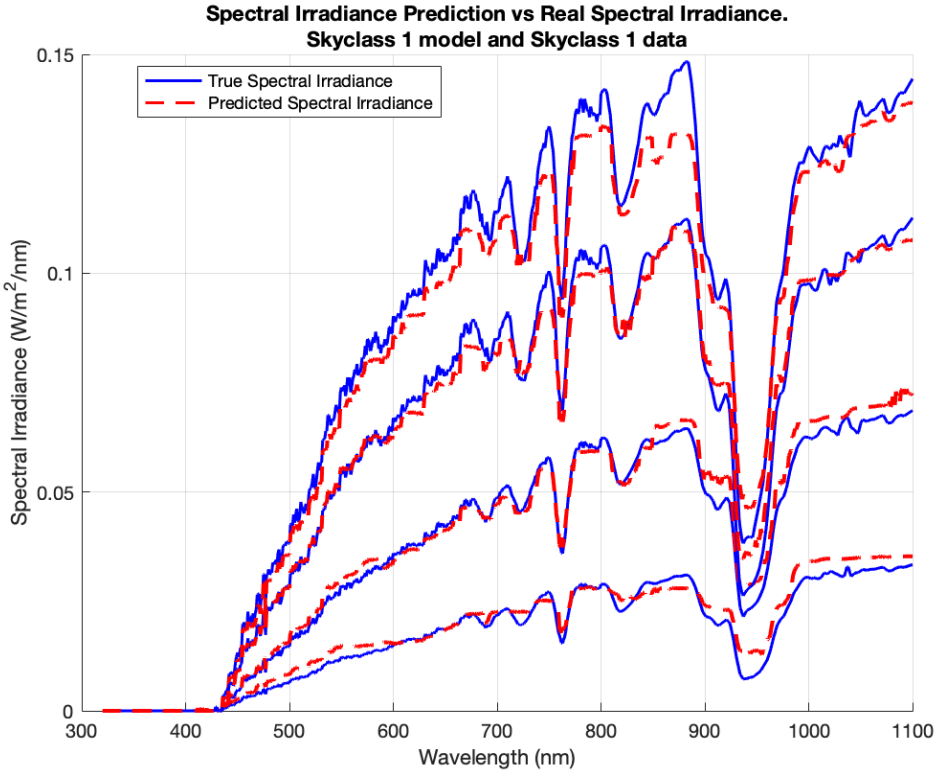

Figure 3.8: Four down-facing spectral irradiance reconstructions predicted using Random Forest Modelling.

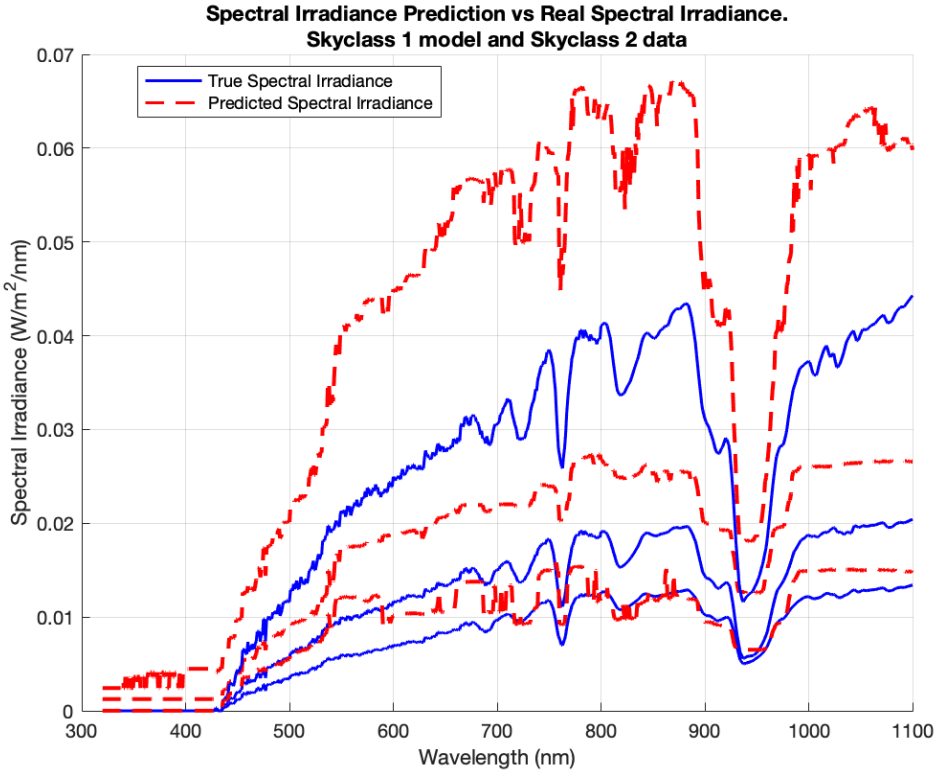

Figure 3.9: Failure case of three down-facing spectral irradiance reconstructions when using SC 2 data in an SC 1 model. The reconstruction is the red dotted lines, as compared to the target spectral irradiance in solid blue.

model is shown in table 3.4. The relative error measurements in band 1 are particularly high as the true values of down-facing spectral irradiance are near-zero in the start of the spectrum. In the remaining two bands, the sensitivity analysis proved that the reconstructions are quite resilient and are still within the acceptable 5% uncertainty bounds until the reflectance spectrum is approximately 20% larger than expected.

3.2.3. Discussion

The results of the spectral albedo reconstruction model were intended to outline whether the real target reflectance spectrum is necessary for the reconstruction of spectral albedo. This could enhance the effectiveness of the device by rendering it more autonomous, reducing the amount of input required by the end-user. However, due to the real values of spectral albedo not being available, the model became overtrained on the same constant output and the errors are near-zero.

In the case of the DFSI model, when the correct Skyclass model and data are used together, the reconstruction error is minimized in skyclasses 1 to 4. Skyclass 1 and 2 are particularly accurate with less than 5% uncertainty in all wavelength bands. This demonstrates that the machine learning method can be a very valuable tool for spectral albedo reconstruction. The major downside of the current model is the Skyclass at the reconstruction time must be extremely accurate, or else the model fails.

Given that the Skyclass of the input data has such a large effect on the reconstruction error. It is a good idea to replace this user input with something measurable, so that the user can find the required inputs from a local weather station. Given that GHI and sun elevation are already incorporated, cloud cover can also be found by using okta, a unit of measurement used to describe the amount of cloud cover at any given time. This information can also be found from a local weather station. In this case, Skyclass should replaced completely by GHI, sun elevation and cloud cover in Okta.

One additional unexpected feature can be observed in the spectral irradiance reconstructions, figure 3.8 and figure 3.9. The dip, due to water vapor absorption of light, in the range of 900-1000nm is present in every DFSI, ML-based reconstruction, while some of the SMARTS-based upward-facing spectral irradiance (UFSI) reconstructions do not accurately represent this 'dip' phenomenon, see figure 3.1. This discovery is relevant because it may provide an ML-approach to simulating the total precipitable water value which the PSO algorithm has trouble consistently predicting, as discussed in section 3.1.4. 'Total precipitable water' is the parameter which determines the amount of absorption in the 900-1000nm range. If ML can be used to estimate this parameter, the reliability of the DFSI reconstruction is improved and reduces effect of one of the systematic errors discussed in section 3.1.4. The PSO algorithm can instead be run with fewer paremeters, reducing the running time of the SMARTS model, or can be used to optimise the value of another atmospheric parameter such as those investigated in section 2.3.2.

Table 3.3: Relative errors of spectral irradiance reconstructions using models trained on data from specific Skyclass data. Mean error and 95% confidence interval is shown.

		Wavelength range [nm]		
		320-590	590-850	850-1100
Skyclass 1	95% confidence interval [%]	[-1, 1.69]	[-0.91, 1.91]	[0.68, 1.7]
	Mean error [%]	0.34	0.5	0.51
Skyclass 2	95% confidence interval [%]	[-4.15, 4.38]	[-1.22, 3.94]	[-4.45, 1.62]
	Mean error [%]	0.11	1.36	-1.41
Skyclass 3	95% confidence interval [%]	[-4.9, 2.18]	[-2.88, 6.01]	[-6.86, 1.52]
	Mean error [%]	-1.36	1.57	-2.67
Skyclass 4	95% confidence interval [%]	[2.46, 7.74]	[1.95, 3.54]	[1.88, 6.73]
	Mean error [%]	5.1	2.74	4.3
Skyclass 5	95% confidence interval [%]	[7.37, 40.84]	[5.04, 36.64]	[10.39, 46.91]
	Mean error [%]	24.11	20.84	28.65

3.3. Albedometer App

3.3.1. Results

The Albedometer App was first sketched on paper and realised in MATLAB App Designer. It features all the inputs required for spectral irradiance and spectral albedo reconstruction, see figure 3.10. The app calls the Windows version of SMARTS and therefore this iteration of the app only functions on Windows devices.

The app is used as follows:

1. Navigate to 'Albedometer Raw File' and select the raw albedometer .csv file from anywhere on the computer.
    - The datafile must contain the data from the desired date and time to be processed.
    - The albedometer file will be loaded and the file name is displayed below in the grey box as confirmation.
2. Select the desired date and time for the reconstruction.
    - The selected date and time will be displayed in the grey box below it.
3. Select the ground material which best describes the material below the albedometer. (The drop down list has multiple options but the spectral albedo model is currently only trained for 'sandy gravel').
4. Select the sky condition at the selected date and time. (One value for each
5. Enter the coordinate location of the albedometer, latitude, longitude and altitude.
6. Select 'Begin Reconstruction'
    - The indicator will turn green to show that the reconstruction is under way. The reconstruction status and start time is printed alongside it (not pictured in figure 3.10)
    - The estimated time for reconstruction is indicated on the right in bold.

    When the reconstruction is complete:
    - The indicator will turn grey and the elapsed time will be displayed.
    - The 'Estimated reconstruction time' will be updated based on the time for the previous reconstruction.
    - The graphs of spectral irradiance and spectral albedo will appear.
    - GHI and sun elevation will be shown.
7. Export the .csv data to your computer by clicking the 'Save as...' button.

Table 3.4: Sensitivity analysis of reflectance spectrum for machine learning model reconstructions. Skyclass 1 model and data was used.

		Wavelength range [nm]		
		320-590	590-850	850-1100
1% increase	95% confidence interval [%]	[0.29, 3.06]	[-0.64, 2.2]	[-0.23, 2.16]
	Mean error [%]	1.67	0.78	0.96
5% increase	95% confidence interval [%]	[2.32, 5.18]	[-0.32, 2.52]	[-0.02, 2.37]
	Mean error [%]	3.75	1.1	1.17
10% increase	95% confidence interval [%]	[7.59, 10.77]	[0.65, 3.50]	[1.53, 3.96]
	Mean error [%]	9.18	2.07	2.75
20% increase	95% confidence interval [%]	[30.01, 34.97]	[3.61, 6.54]	[7.69, 10.32]
	Mean error [%]	32.49	5.08	9

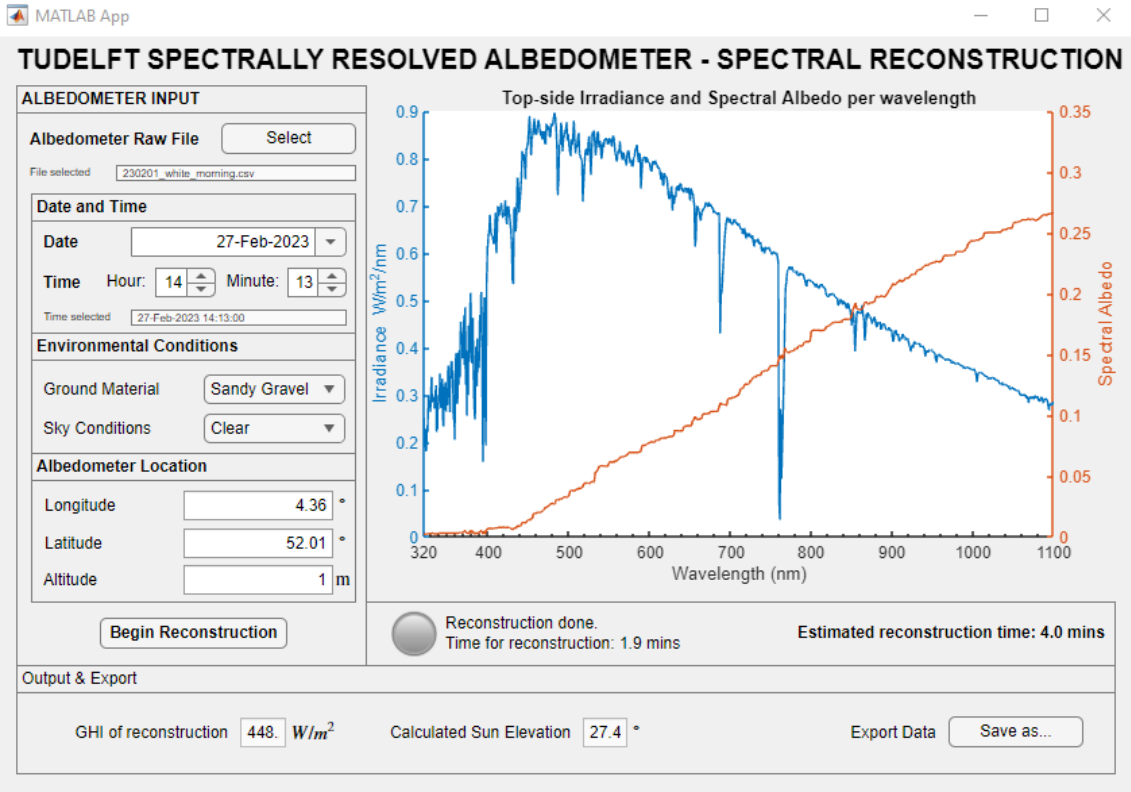

Figure 3.10: Image of the Albedometer App after having completed the spectral irradiance and spectral albedo reconstructions.

3.3.2. Discussion

The Albedometer App improves the usability of the device by centralising all the code required to run the UFSI reconstruction and spectral albedo reconstruction. The user is therefore able to pass from measurement, to tangible reconstruction result with very little time and effort. The design choices and app inputs are explained in section 2.5.

Opening the app, the user is faced with an input panel, where they are able to enter the required inputs for the reconstructions to run. The design is intuitive and well labelled, requiring very few external inputs, which include: the ground material selection, using a drop-down selection tool which automatically imports the required reflectivity spectrum, the sky condition at the selected date and time, which is used to determine the type of ML model used in the reconstruction, and the geographical coordinates of the albedometer device, easily found using online tools.

When the user is ready to run the reconstruction, all the inputs are automatically formatted by app, the reconstructions are run, after which they can be exported to the user's computer.

The current areas for improvement in future iterations would be to add the ability to reconstruct multiple reconstructions at a time, which for example, could help the user develop an understanding of how the spectral irradiance and spectral albedo change over a day. Additionally, a function could be added which would output the effective albedo of a range of standard bi-facial solar panels.

4

Conclusion

The TUDelft spectrally resolved albedometer is a measurement device which aims to accurately reconstruct spectral irradiance and spectral albedo using reconstruction techniques which enable this device to be produced at a lower cost than competitor devices. The current device is capable of measuring the upward-facing and downward-facing irradiance in three wavelength bands and using those inputs to reconstruct the up-facing spectral irradiance.

The three topics of this thesis are outlined as follows:

- Improving the accuracy of the TU Delft albedometer in reconstructing the spectral irradiance at the top side of the device through an updated calibration method.
- Improving the functionality of the device by designing a machine learning model for reconstruction of downward facing spectral irradiance (DFSI) thereby demonstrating the potential for machine learning models in spectral albedo reconstruction.
- Improving the usability of the TU Delft albedometer, wherein a software is designed which centralises the functionalities of the device into one intuitive app.

The first of three research questions introduced in section 1.5 is:

1. **Can the recalibration of the albedometer improve the error measurements of the device or is a physical change to the device required?**

To answer the first research question, the two recommendations given in the previous thesis on this topic [23] are investigated and discussed in section 3.1. The first recommendation is to :

- Recalibrate the albedometer using the recently recalibrated EKO device.

The calibration parameters of the albedometer's upward-facing sensors are calculated according to ISO 9847 - "Calibration of pyranometers by comparison to a reference pyranometer" [14] with the recalibrated EKO device used as the reference pyranometer. Once the calibration factors are acquired, a MATLAB function is written which extracts the relevant irradiance sensor data from the raw albedometer file and applies the calibration factors to the device's sensor measurements.

To better understand the sky conditions under which the spectral irradiance reconstruction performs best, a sky classification code is run using Python, as explained in section 2.1.1, which analyses sky images taken in Delft from September 2022 to May 2023 and classifies them in five Skyclasses, from clear-sky, to overcast conditions. This sky classification is initially used to identify timeframes related to clear sky conditions, a necessity for accurate reconstruction of the spectral irradiance. At the identified timeframes, the measurements of the albedometer's up-facing sensors are used as inputs to a spectral irradiance reconstruction model, the results of which, as shown in section 3.1.1. These results demonstrate that the uncertainty range of the newly calibrated albedometer is reduced in the first and last measured wavelength bands, as shown in table 3.1. Although overall uncertainty range is reduced

following recalibration, the mean errors in the new reconstructions deviate from the previous values, indicating that a systematic error is affecting the results in the first and last wavelength bands: 320-590nm and 850-1100nm.

It is found that the reconstruction in the first and last wavelength bands is particularly affected by the reconstruction of the ranges of 320-400nm and 900-1050nm, see table 3.2, where the atmospheric parameters: trace gas transmittance, ozone reduced pathlength and total precipitable water, contribute most to the absorption of radiance. The latter two parameters are calculated using the PSO algorithm which had been adapted to the previous albedometer calibration. It is therefore proposed that adapting the weights of the parameters in the PSO algorithm to those of the newly calibrated device may eliminate the systematic error.

An additional method to decrease the error in the 900-1000nm range has been identified through the use of machine learning methods for spectral albedo reconstruction section 3.2. It was observed, that in every reconstructed spectrum of DFSI using an ML model, the absorption of radiance in the 900-1000nm range due to total precipitable water in the atmosphere was accurately predicted, see figure 3.8. Training an ML model using real spectral irradiance data and using similar inputs to those of the ML model trained in this report, could enable accurate estimation of the value of total precipitable water. Using this method would ensure that the absorption due to total precipitable water in the 900-1000nm range is consistently reconstructed in the upward-facing spectral irradiance (UFSI) reconstruction using SMARTS, which was not seen when solely using the PSO algorithm to estimate this parameter, see figure 3.1.

The second recommendation is to:

- Investigate whether the trace gas and aerosol transmittance parameters can be optimised to minimise the reconstructed error in the first wavelength band.

To investigate this, spectral irradiance reconstructions are performed for each possible combination of trace gas and aerosol transmittance parameter at a certain date and time. The results presented in section 3.1.3, compare the resulting errors in the first wavelength band, as shown in figure 3.6. The changing of the four aerosol parameters do not demonstrate any significant reduction in reconstruction error. The parameter which most reduces the reconstruction error is the value of tropospheric pollution (Trace gas variable). The level of tropospheric pollution which results in the least error corresponds to 'severe pollution', which is highly unlikely for Delft, the Netherlands, the location where the measurements were taken. Therefore, no conclusive evidence was found to support the hypothesis that changing the trace gas and aerosol parameters will improve the accuracy of the reconstruction in the first wavelength band. This analysis was completed for one specific date and time, more comprehansive solutions could be drawn through repetition of the analysis for other date and time combinations, however this was not possible within the time constraints of this research.

The recalibration methods developed and discussed in this report demonstrate that recalibration of the albedometer has reduced the uncertainty in UFSI reconstruction error. Further research is required to address the identified systematic error which shifts the reconstruction errors out of the desired error bounds. Potential solutions to reduce this systematic error in future work are to adjust the weights of the PSO algorithm to adapt it to the newly calibrated data, and to combine this algorithm with an ML model potentially capable of predicting the value of total precipitable water in the 900-1000nm range. If no further errors persist, physical change to the device is not necessary.

The second research question addressed in this project is:

2. **Can a model be built to reconstruct spectral albedo using the data available to the device?**

Spectral albedo is a per-wavelength measure of how much irradiance is reflected into a down facing sensor, as a proportion of the irradiation incident at the top. Spectral albedo is a multi-dimensional reconstruction which involves external parameters which are not measured by the albedometer. To capture this complex relationship and enable accurate reconstruction of spectral albedo, the Random

Forest machine learning model is chosen, see section 2.4. The original target variable of the ML model was the spectral albedo as measured by two back to back EKO spectroradiometers. In the course of this research, however, availability of spectral albedo data resulted in an alteration of the scope to focus primarily on the reconstruction of down-facing spectral irradiance (DFSI) which features similar daily variation and sky condition dependencies in the spectrum as spectral albedo. The research question will be answered by comparing the error uncertainty of the ML reconstructions to those of a competitor device, the Spectrafy SolarSIM:ALB with $\pm$5% in its wavelength range.

The inputs (features) of the ML model were informed by the results of the upward-facing spectral irradiance (UFSI) reconstruction in changing sky conditions, section 3.1.2. The UFSI results demonstrate that Sun Elevation and GHI have a noticeable effect on reconstruction error and are therefore used as additional inputs to inform the ML model, see table 2.4. Skyclass at the time of reconstruction is also demonstrated to have an effect on reconstruction accuracy and therefore, one ML model is trained for each Skyclass. Furthermore, one of the features of the ML model is the reflectance spectrum of the material under the albedometer. All the training data from the albedometer comes from the the same location, therefore, the ML model is trained for only one material reflectance spectrum, taken from the ASTER spectral library [2], which best imitates the gravelly material under the albedometer. Further ground material types should be implemented in future work, as recommended in chapter 5.

The results of the DFSI reconstructions using machine learning, section 3.2, show that the errors in each wavelength band are successfully maintained below the target error uncertainty of $\pm$5% for skyclass models 1 and 2. Skyclass 3 and 4 also feature an uncertainty of less than $\pm$8% in all wavelength bands. Sensitivity analysis is performed on the the ground material reflectance input, due to the fact that in reality, the reflectance spectrum will vary from the sample spectrum due to differing ground roughness, ground moisture content or other environmental factors. The sensitivity analysis indicates that the error value remains inside the desired $\pm$5% uncertainty for an increase in material reflectance of up to 10%.

The main challenge identified in the model, is the requirement that the correct skyclass model must be used on albedometer data of that same skyclass. If the measurement data belonging to a certain Skyclass is reconstructed using an ML model of a different skyclass, the reconstruction is incorrectly reconstructed, see figure 3.9. In a real life application, this means that the Skyclass prediction selected by the user is of extremely high importance. To address this, it is proposed that the model is trained instead with a more measurable sky-condition such as cloud cover, measured in Okta, which can be gathered accurately from a local weather station. The results shown in figure 3.5a demonstrate how cloud cover affects reconstruction accuracy of UFSI and therefore can help to identify different sky-conditions.

To answer the second research question, the ML model developed to reconstruct the DFSI demonstrates low reconstruction uncertainties. Since the equation for DFSI features many of the same sky condition and ground reflectance dependencies as the spectral albedo, the success of the ML model shows that it is possible reconstruct spectral albedo using the same method.

The third and final research question investigated in this project is:

3. **How can a user interface be designed which simplifies user experience for spectral irradiance and albedo reconstruction?**

The Albedometer App design improves the usability of the device by centralising and automating the code required to prepare the inputs of the reconstructions, as well as by running the reconstructions and allowing the user to export the spectra to their computer.

As mentioned in section 2.5, the design requirements were determined by investigating the potential use-cases of the device and the type of customer that may use the device. It was assumed therefore that the user is technically knowledgeable in operating and installing measurement instruments. Based on these design requirements, a concept sketch was made and the app the final Albedometer App was

realised in MATLAB APP designer, see figure 3.10.

To answer the research question, the app succeeds in simplifying the process of running the reconstructions, streamlining the process from taking the measurement using the albedometer, to having tangible reconstructed outputs of spectral irradiance and spectral albedo with no MATLAB coding knowledge being required.

In conclusion, the project succeeds in answering the three research questions. The reconstruction of UFSI using the albedometer device's sensor measurements now demonstrates an improved error uncertainty of in its wavelength bands and is one step closer to exceeding the error measurements of its competitor devices. The reconstruction of DFSI using machine learning demonstrates the potential for, and created the framework for reconstruction of spectral albedo using machine learning. Finally, the development of the albedometer app streamlines the use of the albedometer's reconstruction models, allowing the user to go from measurement to final output with minimal time and effort. The recommendation in chapter 5 will suggest future work to advance the albedometer device to its full potential as a high accuracy, low cost measurement device.

5

Recommendations

In this chapter, recommendations are made for future work in each of the three results sections discussed in this report. The recommendations aim to improve the accuracy of the Spectral Irradiance Reconstruction, to improve the reliability in the Spectral Albedo reconstructions, and finally to add further functionality to the Albedometer App.

In the Spectral Irradiance Reconstruction results, section 3.1 the uncertainty range of the results was improved in each wavelength band due to the recalibration of the device. The mean error in each of the wavelength bands however, is subject to a systematic error in the first and last wavelength band of the device which pushes the error ranges out of the desired range (as compared to the uncertainties of the EKO device), see table 3.2. The affected error ranges coincide with the atmospheric parameters of 'trace gas concentration', 'ozone reduced pathlength' and 'total precipitable water'. The latter two are calculated by a PSO algorithm, prior to each reconstruction. The recommendations for this section are as follows:

The weights of the PSO algorithm, which determine the optimal values of 'aerosol optical depth at 550nm', 'ozone reduced pathlength' and 'total precipitable water' should be determined based on the new calibration of the albedometer. Additionally, the PSO algorithm sometimes fails to estimate the value of 'total precipitable water' in the atmosphere, meaning that the dip in the 800-900nm range is not reconstructed, see figure 3.1, which directly contributes to the high systematic error in the same range. It is therefore recommended that machine learning (ML) model be used to predict the value of this parameter, as observed in section 3.1, where the 'total precipitable water' dip is consistently well reconstructed. By doing so, the PSO algorithm can more accurately predict the remaining values or even help to predict other parameters such as trace gas concentration.

In the Spectral Albedo Reconstruction results, section 3.2, an ML model is created which accurately reconstructs the down facing spectral irradiance (DFSI), demonstrating that an ML model can be used for spectral albedo reconstruction. As explained in section 2.4, the spectral albedo could not be reconstructed as real spectral albedo data, as measured by two EKO spectroradiometers placed back to back were not installed in time. Assuming that the EKO devices are installed to measure spectral albedo and that sufficient data has been recorded, the first recommendation is to calibrate the the three down-facing sensors of the albedometer as done in section 2.2. It is then recommended to change the target output of the machine learning model to that of the measured spectral albedo.

The ML reconstruction results in this thesis are highly dependant on the user knowing the exact sky condition (Skyclass) at the time of measurement, see section 3.2. To improve the reliability of the ML reconstruction results, it is recommended that model avoid using Skyclass data to reconstruct the results as the value of Skyclass is not easily determined by the end-user. Instead, a measured parameter (from a local weather station) such as cloud cover, measured in Okta, should be tested as an ML model feature to determine whether it can help to determine the sky conditions instead of Skyclass.

In the Albedometer App results section 3.3, an app is designed which improves the usability of the device by streamlining the process of gathering and processing data for the reconstruction of up-facing spectral irradiance (UFSI) and spectral albedo. Some recommendations for future work include the ability to reconstruct effective albedo for a range of standard Bifacial PV cells. This would allow bifacial PV system planners to more easily find relevant information for their projects. Finally, it is recommended that a function is added to the Albedometer App which allows the user to reconstruct the UFSI and spectral albedo for multiple times in one go: for example, at multiple times over the course of the day, which would help the user to understand the daily variation of spectral irradiance and albedo over the course of the day.

References

[1] JJRE Appelbaum. “Bifacial photovoltaic panels field”. In: *Renewable Energy* 85 (2016), pp. 338–343.

[2] ASTER. *ASTER spectral library*. Has now become ECOSTRESS Spectral Library. 2018. URL: https://asterweb.jpl.nasa.gov/index.asp.

[3] Inc. Campbell Scientific. *EKO MS-700 Spectroradiometer Interfaced with a CR3000 Datalogger*. Accessed on: 23-09-2023. 2018. URL: https://s.campbellsci.com/documents/us/technical-papers/ms700-to-cr3000.pdf.

[4] Anton Driesse and Willem Zaaiman. “Characterization of Global Irradiance Sensors for use with PV Systems”. In: June 2015. DOI: 10.1109/PVSC.2015.7356004.

[5] E. Enríquez et al. “New strategy to mitigate urban heat island effect: Energy saving by combining high albedo and low thermal diffusivity in glass ceramic materials”. In: *Solar Energy* 149 (2017), pp. 114–124. ISSN: 0038-092X. DOI: https://doi.org/10.1016/j.solener.2017.04.011. URL: https://www.sciencedirect.com/science/article/pii/S0038092X17302955.

[6] R. Guerrero-Lemus et al. “Bifacial solar photovoltaics – A technology review”. In: *Renewable and Sustainable Energy Reviews* 60 (2016), pp. 1533–1549. ISSN: 1364-0321. DOI: https://doi.org/10.1016/j.rser.2016.03.041. URL: https://www.sciencedirect.com/science/article/pii/S1364032116002768.

[7] Chris Gueymard. “Development and performance assessment of a clear sky spectral radiation model”. In: Jan. 1993, pp. 433–438.

[8] Christian A. Gueymard. *SMARTS code, version 2.9.2 USER’S MANUAL*. Solar Consulting Services, 2003.

[9] Odelle L. Hadley and Thomas W. Kirchstetter. “Black-carbon reduction of snow albedo”. In: *Nature Climate Change* (2012). DOI: 10.1038/nclimate1433.

[10] IBM. *What is machine learning?* Accessed on: 28-09-2023. 2023. URL: https://www.ibm.com/topics/machine-learning.

[11] IBM. *What is overfitting?* Accessed on: 28-09-2023. 2023. URL: https://www.ibm.com/topics/overfitting.

[12] IBM. *What is random forest?* Accessed on: 28-09-2023. 2023. URL: https://www.ibm.com/topics/random-forest.

[13] “International Technology Roadmap for Photovoltaic (ITRPV)”. In: (Apr. 2023).

[14] *Solar energy — Calibration of pyranometers by comparison to a reference pyranometer*. Standard. Geneva, CH: International Organization for Standardization, 1992.

[15] Mark Z. Jacobson. “Climate response of fossil fuel and biofuel soot, accounting for soot’s feedback to snow and sea ice albedo and emissivity”. In: *Journal of Geophysical Research: Atmospheres* 109.D21 (2004). DOI: https://doi.org/10.1029/2004JD004945. URL: https://agupubs.onlinelibrary.wiley.com/doi/abs/10.1029/2004JD004945.

[16] Markku Järvelä, Kari Lappalainen, and Seppo Valkealahti. “Cloud Enhancement Phenomenon and Its Effect on PV Generators”. In: Sept. 2018.

[17] Takeyoshi Kato. “Chapter 4 - Prediction of photovoltaic power generation output and network operation”. In: *Integration of Distributed Energy Resources in Power Systems*. Ed. by Toshihisa Funabashi. Academic Press, 2016, pp. 77–108. ISBN: 978-0-12-803212-1. DOI: https://doi.org/10.1016/B978-0-12-803212-1.00004-0. URL: https://www.sciencedirect.com/science/article/pii/B9780128032121000040.

[18] Annanta Kaul. *Design and Fabrication of an Irradiance Sensor for Bifacial PV*. 2020.

[19] H. Lee and J. Romero. “Climate Change 2023: Synthesis Report. Contribution of Working Groups I, II and III to the Sixth Assessment Report of the Intergovernmental Panel on Climate Change”. In: (2023). DOI: 10.59327/IPCC/AR6-9789291691647.

[20] Philip Lewis and M. Barnsley. “Influence of the sky radiance distribution on various formulations of the Earth surface albedo”. In: *Proc. Conf. Phys. Meas. Sign. Remote Sens.* (Jan. 1994).

[21] Victor Arturo Martinez Lopez et al. “Using sky-classification to improve the short-term prediction of irradiance with sky images and convolutional neural networks”. In: May 2023.

[22] Yunan Lu et al. “Albedo of Pervious Concrete and Its Implications for Mitigating Urban Heat Island”. In: *Sustainability* 15.10 (2023). ISSN: 2071-1050. DOI: 10.3390/su15108222. URL: https://www.mdpi.com/2071-1050/15/10/8222.

[23] Wijnand Meines. *Spectral irradiance reconstruction model In MATLAB utilizing a spectrally resolved albedometer*. 2022.

[24] Anne W. Nolin and Julienne Stroeve. “The changing albedo of the Greenland ice sheet: implications for climate modeling”. In: *Annals of Glaciology* 25 (1997), pp. 51–57. DOI: 10.3189/S0260305500013793.

[25] Ana Romero Olvera. *Bio-Inspired Design and Fabrication of a Spectrally Resolved Albedometer*. 2021.

[26] Silvana Ayala Pelaez et al. “Comparison of Bifacial Solar Irradiance Model Predictions With Field Validation”. In: *IEEE Journal of Photovoltaics* 9.1 (2019), pp. 82–88. DOI: 10.1109/JPHOTOV.2018.2877000.

[27] J. Pérez Oria and G. Sala. “A good combination: Tracking of the sun in polar axis and bifacial photovoltaic modules”. In: *Solar & Wind Technology* 5.6 (1988), pp. 629–636. ISSN: 0741-983X. DOI: https://doi.org/10.1016/0741-983X(88)90060-4. URL: https://www.sciencedirect.com/science/article/pii/0741983X88900604.

[28] Muhammad Hussnain Riaz et al. “The optimization of vertical bifacial photovoltaic farms for efficient agrivoltaic systems”. In: *Solar Energy* 230 (2021), pp. 1004–1012. ISSN: 0038-092X. DOI: https://doi.org/10.1016/j.solener.2021.10.051. URL: https://www.sciencedirect.com/science/article/pii/S0038092X21009087.

[29] Nicholas Riedel-Lyngskaer et al. “The effect of spectral albedo in bifacial photovoltaic performance”. In: (2021). DOI: 10.11583/DTU.14695437.v1. URL: http://creativecommons.org/licenses/by/4.0/.

[30] Eric P. Shettle and Robert W. Fenn. “Models for the aerosols of the lower atmosphere and the effects of humidity variations on their optical properties”. In: 1979. URL: https://api.semanticscholar.org/CorpusID:129284964.

[31] Spectrafy. *SolarSIM-ALB*. Accessed on: 23-09-2023. 2021. URL: https://www.spectrafy.com/products/solarsim-alb.

[32] Viktar Tatsiankou et al. “Reconstruction of solar spectral resource using limited spectral sampling for concentrating photovoltaic systems”. In: *Photonics North 2013*. Ed. by Pavel Cheben et al. Vol. 8915. International Society for Optics and Photonics. SPIE, 2014, p. 891506. DOI: 10.1117/12.2033613. URL: https://doi.org/10.1117/12.2033613.

[33] Gijs van Urk. *Improving irradiance prediction by using classification of sky images and deep learning*. 2022.

[34] Jie Wang. “An Intuitive Tutorial to Gaussian Processes Regression”. In: Sept. 2020.

[35] Jiachuan Yang, Zhi-Hua Wang, and Kamil E. Kaloush. “Environmental impacts of reflective materials: Is high albedo a ‘silver bullet’ for mitigating urban heat island?” In: *Renewable and Sustainable Energy Reviews* 47 (2015), pp. 830–843. ISSN: 1364-0321. DOI: https://doi.org/10.1016/j.rser.2015.03.092. URL: https://www.sciencedirect.com/science/article/pii/S1364032115002452.

[36] Hesan Ziar et al. “A comprehensive albedo model for solar energy applications: Geometric spectral albedo”. In: *Applied Energy* 255 (2019), p. 113867. ISSN: 0306-2619. DOI: https://doi.org/10.1016/j.apenergy.2019.113867. URL: https://www.sciencedirect.com/science/article/pii/S0306261919315545.

[37] Kipp & Zonen. *SOLYS2 sun tracker*. Accessed on: 23-09-2023. 2023. URL: https://www.kippzonen.com/Product/20/SOLYS2-Sun-Tracker.

A

Raw Sample Data

Cloud Dataframe / Sky classification files

timeStamp	GHI	Temp	elevation	GHI0	image	kc	CloudCover	skyclass
01/02/2023 10:25	72	8	13.4727909	191.03926	O:\LucasBun	0.37688588	0.42923619	5
01/02/2023 10:26	71	8	13.5653687	192.682243	O:\LucasBun	0.36848232	0.41114393	5
01/02/2023 10:27	81	8	13.657459	194.318159	O:\LucasBun	0.41684215	0.44316336	5
01/02/2023 10:28	90	8	13.7490599	195.946922	O:\LucasBun	0.45930806	0.51270281	5
01/02/2023 10:29	98	8	13.8401692	197.568446	O:\LucasBun	0.49603063	0.59225598	2
01/02/2023 10:30	106	8	13.9307848	199.182643	O:\LucasBun	0.53217488	0.66887492	2
01/02/2023 10:31	111	8	14.0209046	200.789432	O:\LucasBun	0.55281794	0.67087165	2
01/02/2023 10:32	116	8	14.1105266	202.388727	O:\LucasBun	0.57315445	0.72479559	2
01/02/2023 10:33	125	8	14.1996487	203.980449	O:\LucasBun	0.61280383	0.77950934	2
01/02/2023 10:34	135	8	14.2882688	205.564515	O:\LucasBun	0.65672813	0.84909187	3
01/02/2023 10:35	159	8	14.3763849	207.140846	O:\LucasBun	0.76759366	0.92233551	3
01/02/2023 10:42	143	8	14.9789117	217.95206	O:\LucasBun	0.65610759	0.99514905	3
01/02/2023 10:44	92	8	15.1464089	220.967016	O:\LucasBun	0.41635173	0.99454934	4
01/02/2023 10:45	96	8	15.2293718	222.461804	O:\LucasBun	0.43153475	0.994416	3
01/02/2023 10:46	99	8	15.3118081	223.948039	O:\LucasBun	0.44206683	0.99396537	3
01/02/2023 10:47	97	8	15.393716	225.425651	O:\LucasBun	0.43029708	0.99338413	3
01/02/2023 10:48	93	8	15.4750932	226.894573	O:\LucasBun	0.40988199	0.99312907	4
01/02/2023 10:49	82	8	15.5559379	228.354736	O:\LucasBun	0.35909043	0.99261963	4
01/02/2023 10:50	68	8	15.6362481	229.806074	O:\LucasBun	0.29590167	0.99179427	4
01/02/2023 10:51	56	8	15.7160217	231.248521	O:\LucasBun	0.24216371	0.9912691	4

Figure A.1: Sample data from the sky classifier code explained in section 2.1.1

Raw Albedometer data file

Time	Date and Time	TempTop	IrrHMtop	IrrLPtop	IrrNFtop	TempBTM	IrrHMBTM	IrrLPBTM	IrrNFBTM
1646654715	07/03/2022 13:05:15	15.64	5.77	7.72	16.97	12.89	50.85	34.6	70.83
1646654716	07/03/2022 13:05:16	15.56	5.92	7.72	17.17	12.97	50.82	34.59	71.22
1646654717	07/03/2022 13:05:17	15.54	5.79	7.71	16.94	12.99	50.84	34.5	71.35
1646654718	07/03/2022 13:05:18	15.53	5.87	7.66	17.17	13.01	50.84	34.53	71.22
1646654720	07/03/2022 13:05:20	15.52	6.01	7.74	18.11	13	49.96	33.89	70.15
1646654721	07/03/2022 13:05:21	15.51	5.94	7.77	17.88	12.96	49.95	34.01	69.66
1646654722	07/03/2022 13:05:22	15.51	5.6	7.68	16.68	12.97	50.8	34.54	71.29
1646654723	07/03/2022 13:05:23	15.5	5.83	7.71	16.84	12.99	50.83	34.51	71.39
1646654724	07/03/2022 13:05:24	15.49	6	7.69	16.97	12.96	50.83	34.56	71.26
1646654725	07/03/2022 13:05:25	15.5	6.05	7.77	17.82	12.97	50.83	34.56	71.39
1646654726	07/03/2022 13:05:26	15.49	5.43	7.72	16.84	13.01	50.88	34.56	71.42
1646654728	07/03/2022 13:05:28	15.69	94.58	54.3	129.94	12.82	52.02	35.31	72.17
1646654729	07/03/2022 13:05:29	15.93	216.98	118.19	282.07	12.62	51.78	34.87	72.27
1646654730	07/03/2022 13:05:30	15.91	216.88	118.14	281.81	12.61	47.41	31.77	67.35
1646654731	07/03/2022 13:05:31	15.91	216.85	118.19	281.75	12.61	44.96	30.05	65.03
1646654732	07/03/2022 13:05:32	15.94	216.84	118.13	281.72	12.61	44.9	30.02	65.03
1646654733	07/03/2022 13:05:33	15.92	216.84	118.17	282.04	12.6	44.88	29.94	65.03
1646654734	07/03/2022 13:05:34	15.9	216.88	118.22	282.14	12.61	45.23	29.93	65.03
1646654736	07/03/2022 13:05:36	15.92	216.96	118.2	282.24	12.61	45.71	30.12	65.23

Figure A.2: Raw Albedometer file. Time is in UNIX time format. 'Irr' columns refer to Irradiance measurements of each sensor range for top and bottom of the device. Temp refers to internal operating temperatures on top and bottom of device.

EKO device files

idSpecoverview	Type	RecTime	Spec_start	Spec_stop	Exposure_time	PAR	Photon	Lux
543748	1	02/01/2023 09:54	139196122	139196377	1000	14.78	67.8	3617.4
543749	1	02/01/2023 09:55	139196378	139196633	1000	14.74	67.5	3606.4
543750	1	02/01/2023 09:56	139196634	139196889	1000	14.55	66.6	3557.2
543751	1	02/01/2023 09:57	139196890	139197145	1000	14.13	64.7	3452.6
543752	1	02/01/2023 09:58	139197146	139197401	1000	13.61	62.3	3322.1
543753	1	02/01/2023 09:59	139197402	139197657	1000	13.25	60.6	3230
543754	1	02/01/2023 10:00	139197658	139197913	1000	12.98	59.3	3158.9
543755	1	02/01/2023 10:01	139197914	139198169	1000	12.67	57.8	3080.6
543756	1	02/01/2023 10:02	139198170	139198425	1000	12.4	56.6	3011.3
543757	1	02/01/2023 10:03	139198426	139198681	1000	12.01	54.7	2913.8
543758	1	02/01/2023 10:04	139198682	139198937	1000	11.56	52.6	2801.3
543759	1	02/01/2023 10:05	139198938	139199193	1000	10.9	49.6	2638.9
543760	1	02/01/2023 10:06	139199194	139199449	1000	10.27	46.7	2484.2
543761	1	02/01/2023 10:07	139199450	139199705	1000	9.87	44.9	2386
543762	1	02/01/2023 10:08	139199706	139199961	1000	9.74	44.3	2352.2
543763	1	02/01/2023 10:09	139199962	139200217	1000	9.54	43.3	2301.6
543764	1	02/01/2023 10:10	139200218	139200473	1000	9.22	41.8	2219.3
543765	1	02/01/2023 10:11	139200474	139200729	1000	8.85	40.1	2128.2
543766	1	02/01/2023 10:12	139200730	139200985	1000	8.53	38.6	2046.8
543767	1	02/01/2023 10:13	139200986	139201241	1000	8.26	37.3	1974.4
543768	1	02/01/2023 10:14	139201242	139201497	1000	7.97	35.9	1897.3
543769	1	02/01/2023 10:15	139201498	139201753	1000	7.69	34.5	1818.5
543770	1	02/01/2023 10:16	139201754	139202009	1000	7.49	33.5	1758.2

Figure A.3: File of specoverview, originating from the EKO device, which references the start (Spec_start) and end (Spec_stop) indices for the time and day of the desired spectral irradiance. Exposure time is measured in (ms), PAR is Photosynthetically Active radiation, measured in (W/m^2), Photon is photon intensity measured in ($\mu mol/m^2/s$), Lux indicates the illuminance (lx)

idspecdata	wavelength	spec_irr
139196120	1139.4	0
139196121	1142.6	0
139196122	302.2	0
139196123	305.5	0
139196124	308.8	0
139196125	312.1	0
139196126	315.4	0
139196127	318.8	0
139196128	322.1	0
139196129	325.4	0
139196130	328.7	0
139196131	332	0
139196132	335.4	0
139196133	338.7	0
139196134	342	0
139196135	345.3	0
139196136	348.6	14.848
139196137	352	16.045
139196138	355.3	16.61
139196139	358.6	17.087
139196140	361.9	18.618
139196141	365.3	20.667
139196142	368.6	21.755

Figure A.4: File of specdata which shows the spectral irradiance ($W/m^2/nm$) at each wavelength (nm), between the two ID values that identify a date and time in specoverview figure A.3.

Ground material reflectivity file as imported from ASTER spectral library [2]

```
Name: Gray/dark brown extremely stoney coarse sandy
Type: soil
X Units: Wavelength (micrometers)
Y Units:Reflectance (percent)

14.0112       1.9641
13.9734       2.0002
13.9359       2.0259
13.8985       2.0410
13.8614       2.0530
13.8244       2.0693
13.7876       2.0925
13.7511       2.1189
13.7147       2.1404
13.6785       2.1550
13.6425       2.1648
13.6067       2.1665
13.5711       2.1609
13.5356       2.1501
13.5004       2.1370
13.4653       2.1240
13.4304       2.1167
13.3957       2.1213
13.3612       2.1374
13.3269       2.1577
13.2927       2.1768
13.2587       2.1916
13.2249       2.2041
13.1912       2.2131
13.1577       2.2263
13.1244       2.2517
13.0913       2.2891
13.0583       2.3347
13.0255       2.3877
12.9929       2.4485
12.9604       2.5139
12.9281       2.5752
12.8959       2.6291
12.8639       2.6702
12.8321       2.6892
12.8004       2.6794
```

Figure A.5: File of ground material reflectivity per wavelength. Left column is x and indicates wavelength (μm), right column is Y and indicates the reflectivity (%) at the corresponding wavelength.

B

PVMDalbedometer.m code - New methods

This appendix is used to show the the new methods added to the PVMDalbedometer.m Class file to streamline the process of preparing SMARTS and spectral irradiance reconstructions and the method called to run the spectral albedo reconstruction.

Initialisation function, called using obj = PVMDalbedometer(). Loads the default values of geographical location, alitude, predominant alebdo and time zone required for the SMARTS reconstruction. Defines the values of temperature coefficients the updated calibration factors. At this point in the project, the calibration factors for the top sensors are assumed to be same for the bottom sensors.

```
function obj= PVMDalbedometer() %TODO:
    %PVMDalbedometer creates an object of class PVMDalbedometer.

    obj.latitude =  52.011902;
    obj.longitude = 4.36026;
    obj.altitude = 1;
    obj.PredominantAlbedo = 0.18; % Annata thesis page 75
    obj.TimeZone = 1;

    %Ananta Thesis page 60
    obj.TemperatureCoefficientTOP320_1100 = -0.013;
    obj.TemperatureCoefficientTOP590_1100 = -0.108;
    obj.TemperatureCoefficientTOP850_1100 = 0.054;

    %Anants Thesis assumed same temp dependency page 60
    obj.TemperatureCoefficientBTM320_1100 = -0.013;
    obj.TemperatureCoefficientBTM590_1100 = -0.108;
    obj.TemperatureCoefficientBTM850_1100 = 0.054;

    %Calibration factors of the top side sensors
    obj.CalibrationFactorTOP320_1100 = 1.5872;
    obj.CalibrationFactorTOP590_1100 = 1.2886;
    obj.CalibrationFactorTOP850_1100 = 0.8025;

    %Calibration factors of the bottom side sensors
    %Temporarily assumed to be the same as the top side.
    obj.CalibrationFactorBTM320_1100 = 1.5872;
    obj.CalibrationFactorBTM590_1100 = 1.2886;
    obj.CalibrationFactorBTM850_1100 = 0.8025;

 end
```

Class method which imports the object, the desired date and time 'Time' for reconstruction in datetime format and 'albFile' the filepath for the raw albedometer file which contains the desired information. Outputs albSensorValues, needed for the ML modelling of the spectral albedo, and GHI, required as an input for SMARTS reconstruction.

```
function [albSensorValues,GHI]=calibrateSensorsGetGHI(obj,Time,albFile)
    %Calibrate top and bottom sensors based on the calibration
    %factors. Then calculate GHI

    %albFile = '230201_white_morning.csv'
    %Time = datetime(2023,02,03,11,00,00)

    alb_data = albFile;

    % Check if albFile is a table and has the required variable names
    if ~ istable(alb_data)

        % Fetch Albedometer data file
        alb_data = readtable(alb_data); %220907-WHITE-morning

    end

    %Renaming Variable names in alb_data
    new_names = {'Time','DateAndTime','TempTop','IrrHMtop','IrrLPtop',...
        'IrrNFtop','TempBTM','IrrHMBTM','IrrLPBTM','IrrNFBTM'};
    alb_data.Properties.VariableNames = new_names;

    % Find albedometer time value closest to the EKO measurement time.
    [time_check, index] = min(abs(alb_data.DateAndTime - Time));

    if Time - abs(time_check) <= Time - seconds(2)
        error('Error: Required time: %s is not within the data range', datestr(Time))
    end

    %% TOP Calibration
    % Apply temperature calibration
    NF = alb_data.IrrNFtop(index) + obj.TemperatureCoefficientTOP320_1100 * (alb_data.TempTop
        (index) - 25); %320-1100nm
    HM = alb_data.IrrHMtop(index) + obj.TemperatureCoefficientTOP590_1100 * (alb_data.TempTop
        (index) - 25); %590-1100nm
    LP = alb_data.IrrLPtop(index) + obj.TemperatureCoefficientTOP850_1100 * (alb_data.TempTop
        (index) - 25); %850-1100nm

    %Apply Calibration factors
    NF = NF * obj.CalibrationFactorTOP320_1100;
    HM = HM * obj.CalibrationFactorTOP590_1100;
    LP = LP * obj.CalibrationFactorTOP850_1100;

    albSensorsTop = [NF,HM,LP];

    %% BOTTOM Calibration
    %Apply temperature calibration
    NFbtm = alb_data.IrrNFBTM(index) + obj.TemperatureCoefficientBTM320_1100 * (alb_data.
        TempBTM(index) - 25); %320-1100nm
    HMbtm = alb_data.IrrHMBTM(index) + obj.TemperatureCoefficientBTM590_1100 * (alb_data.
        TempBTM(index) - 25); %590-1100nm
    LPbtm = alb_data.IrrLPBTM(index) + obj.TemperatureCoefficientBTM850_1100 * (alb_data.
        TempBTM(index) - 25); %850-1100nm

    %Apply Calibration factors
    NFbtm = NFbtm * obj.CalibrationFactorBTM320_1100;
    HMbtm = HMbtm * obj.CalibrationFactorBTM590_1100;
    LPbtm = LPbtm * obj.CalibrationFactorBTM850_1100;

    albSensorsBtm = [NFbtm,HMbtm,LPbtm];

    albSensorValues = [albSensorsTop;albSensorsBtm];

    GHI = [];
    GHI(1)= albSensorsTop(1); %320-1100 nm
```

```
    GHI(2)= albSensorsTop(1)-albSensorsTop(2); %320-590 nm
    GHI(3)= albSensorsTop(2)-albSensorsTop(3); %590-850 nm
    GHI(4)= albSensorsTop(3); %850-1100 nm

end
```

Class Method which runs the machine learning model for spectral reconstruction. The inputs are the object, the 'Time' is the date and time of the reconstruction desire in 'datetime' format, SmartsSpectrum is the output of the SMARTS reconstruction, albSensorValues and GHI are the outputs prepared in the 'calibrateSensorsGetGHI method, reflectivityFilePath is the filepath of the desired material reflectivity file, see appendix A and MLModel is the Machine learning model used for the prediction in .mat format. The outputs are the specAlbSpectrum, the spectrum of the reconstructed spectral albedo and sunEl, the calculated sun elevation at that time.

```
function [specAlbSpectrum, sunEl]=reconstructSpecAlbedo(obj,Time,SmartsSpectrum,
    albSensorValues,GHI,reflectivityFilePath,MLModel)
    %This file prepares the input file for the ML model given the
    % provided variables then executes the spectral albedo
    % reconstruction.

    %SmartsSpectrum comes directly from reconstructSpectrum
    %albSensorValues and GHI come directly from calibrateSensorsGetGHI
    %reflectivityFilePath is the filepath to the ASTER reflectivity
    %file which is a .txt.
    %MLModel is the Machine Learning Model in 'TreeBagger' format

    % Get the reflectivity spectrum of the bottom surface
    reflectivitySpectrum = extractReflectivity(reflectivityFilePath);

    AsterLambda = table2array(reflectivitySpectrum(:,1));
    AsterSpectrum = table2array(reflectivitySpectrum(:,2));

    % Get the reconstructed SMARTS array
    % RENAME VARIABLENAME EKO TO SMARTS!!!!!
    EKOLambda = SmartsSpectrum.Wvlgth;
    EKOSpectrum = SmartsSpectrum.Global_horizn_irradiance;

    %% Extrapolate SMARTS reconstruction and reflectivity
    [EKOSpectrum, EKOLambda] = linearExtrapolation(EKOSpectrum, EKOLambda, 10, 300, 1120);

    % Convert negative values to zero
    EKOSpectrum(EKOSpectrum < 0) = 0;

    %Extrapolate Aster data
    AsterSpectrum(AsterLambda > 1200) = [];
    AsterLambda(AsterLambda > 1200) = [];

    % Combine AsterLambda and AsterSpectrum into a matrix
    AsterData = [AsterSpectrum, AsterLambda];

    % Sort the matrix based on the first column (AsterLambda)
    AsterData = sortrows(AsterData, 2);

    [AsterSpectrum,AsterLambda] = linearExtrapolation(AsterData(:,1), AsterData(:,2), 2, 300,
        []);

    %% Resample datasets to have same x values

    % Select min and max points for resampling
    minLambda = 320; %Min and Max value measured by Albedometer
    maxLambda = 1100;

    % Create a common set of x-points
    % Number of desired x-points - minimum sample size of EKO or Aster
    numPoints = 500;
    commonLambda = linspace(minLambda, maxLambda, numPoints)';

    % Interpolate the data series
    smartsResample = interp1(EKOLambda, EKOSpectrum, commonLambda, 'linear');
    reflectionResample = interp1(AsterLambda, AsterSpectrum, commonLambda, 'linear');
```

```
55
56      %% Sun Elevation Calculation
57
58      LocationStruct.latitude = obj.latitude;
59      LocationStruct.longitude = obj.longitude;
60      LocationStruct.altitude = obj.altitude;
61
62      TimeStruct.year = Time.Year;
63      TimeStruct.month = Time.Month;
64      TimeStruct.day = Time.Day;
65      TimeStruct.hour = Time.Hour;
66      TimeStruct.minute = Time.Minute;
67      TimeStruct.second = Time.Second;
68
69      % This is the lazy way to do this, in reality, the time changes
70      % on the last weekend of March and October.
71      if TimeStruct.month > 3 && month < 11
72          TimeStruct.UTCOffset = 2;
73      else
74          TimeStruct.UTCOffset = 1;
75      end
76
77      % obj is passed into the function to provide location coords.
78      [~, sunEl] = pvl_spa(TimeStruct, LocationStruct);
79
80      %% Albdeo band values
81
82      %Calculate measured albedo values
83      albSensorsBtm = albSensorValues(2,:);
84      GHItop = GHI(1,:);
85
86      GHIbtm = [];
87      GHIbtm(1)= albSensorsBtm(1); %320-1100 nm
88      GHIbtm(2)= albSensorsBtm(1)-albSensorsBtm(2); %320-590 nm
89      GHIbtm(3)= albSensorsBtm(2)-albSensorsBtm(3); %590-850 nm
90      GHIbtm(4)= albSensorsBtm(3); %850-1100 nm
91
92      %Calculate measured albedo values
93      measuredAlbedo = GHIbtm ./ GHItop;
94
95      % Calculate band widths
96      band1 = sum(commonLambda >= min(commonLambda) & commonLambda < 590);
97      band2 = sum(commonLambda >= 590 & commonLambda < 850);
98      band3 = sum(commonLambda >= 850 & commonLambda <= 1100);
99
100     % Measured Albedo value from Albedometer and change length to sensor ranges
101     band1Top = repmat(GHItop(2),band1,1);
102     band2Top = repmat(GHItop(3),band2,1);
103     band3Top = repmat(GHItop(4),band3,1);
104
105     % Measured Albedo value from Albedometer and change length to sensor ranges
106     band1Btm = repmat(GHIbtm(2),band1,1);
107     band2Btm = repmat(GHIbtm(3),band2,1);
108     band3Btm = repmat(GHIbtm(4),band3,1);
109
110     % Measured Albedo value from Albedometer and change length to sensor ranges
111     band1Alb = repmat(measuredAlbedo(2),band1,1);
112     band2Alb = repmat(measuredAlbedo(3),band2,1);
113     band3Alb = repmat(measuredAlbedo(4),band3,1);
114
115     %% Update Final Variables
116
117     bandAlbedo = [band1Alb;band2Alb;band3Alb];
118     wavelength = commonLambda;
119     sunElevation = repmat(sunEl(1),length(commonLambda),1); % Constant in one wavelength
            range
120     bandTop = [band1Top;band2Top;band3Top];
121     bandBottom = [band1Btm;band2Btm;band3Btm];
122     smartsArray = smartsResample;
123     reflectionArray = reflectionResample;
124
```

```
125     specAlbInput = [bandAlbedo,wavelength,sunElevation,bandTop,...
126         bandBottom,smartsArray,reflectionArray];
127 
128     % Reconstruct Specreal Albedo using ML Model
129     predictedSpectralAlbedo = predict(MLModel, specAlbInput);
130 
131     specAlbSpectrum = [wavelength,predictedSpectralAlbedo];
132 
133 end
134 end
```